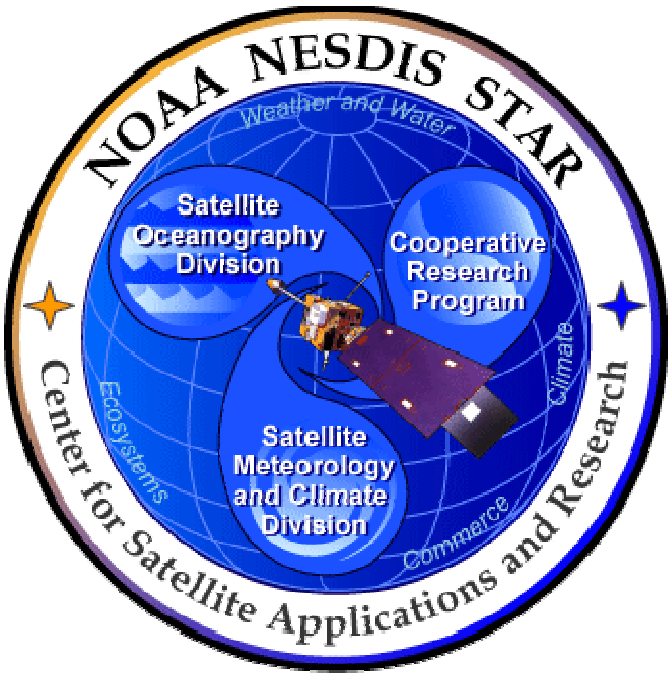

NOAA NESDIS
CENTER for SATELLITE APPLICATIONS and RESEARCH

GOES-R Advanced Baseline Imager (ABI) Algorithm Theoretical Basis Document For Nighttime Cloud Optical Depth, Cloud Particle Size, Cloud Ice Water Path, and Cloud Liquid Water Path

Patrick Minnis, NASA Langley Research Center
Patrick W. Heck, UW-Madison/CIMSS

Version 2.0
July 15, 2010

TABLE OF CONTENTS

LIST OF FIGURES

LIST OF TABLES

LIST OF ACRONYMS

ABI - Advanced Baseline Imager
AERI – Atmospheric Emitted Radiance Interferometer
AIT - Algorithm Integration Team
AMF – ARM Mobile Facility
ARM – Atmospheric Radiation Measurement
ATBD - algorithm theoretical basis document
AVHRR - Advanced Very High Resolution Radiometer
AWG - Algorithm Working Group
BTD - Brightness Temperature Difference
CALIPSO - Cloud-Aerosol Lidar and Infrared Pathfinder Satellite Observations
CARL - Climate Research Facility Raman Lidar
CERES - Clouds and the Earth's Radiant Energy System
CIMSS - Cooperative Institute for Meteorological Satellite Studies
COD - Cloud Optical Depth
CONUS - Continental United States
CPS - Cloud Particle Size
CTT - Cloud Top Temperature
F&PS - Function and Performance Specification
GEOPROF - Geometrical Profiling algorithm
GFS - Global Forecast System
GOES - Geostationary Operational Environmental Satellite
IRR - Imaginary Indices of Refraction
IWP - Ice Water Path
LWP - Liquid Water Path
MODIS - Moderate Resolution Imaging Spectroradiometer
NASA - National Aeronautics and Space Administration
NCOMP - Nighttime Cloud Optical and Microphysical Properties
NWP - Numerical Weather Prediction
PFAAST - Pressure layer Fast Algorithm for Atmospheric Transmittances
RO - Radar Only
RTM - Radiative Transfer Model
SEVIRI - Spinning Enhanced Visible and Infrared Imager
SGP - Southern Great Planes
SIRTA - Site Instrumental de Recherche par Teledetection Atmospheric
SIST - Shortwave-infrared Infrared Split-window Technique
SSEC - Space science and Engineering Center
TOA - Top of Atmosphere
UW - University of Wisconsin

ABTRACT

The Nighttime Cloud Optical and Microphysical Property Algorithm Theoretical Basis Document details the physical basis for the algorithm to be used to retrieve nighttime water and ice cloud optical depth, particle size and liquid or ice water path from imagery taken by the Advanced Baseline Imager aboard GOES-R. The algorithm is based primarily on the Solar Infrared Solar-infrared Technique from NASA Langley Research Center, but as been adapted to utilize upstream GOES-R products and to function in the GOES-R framework. Sufficient information is provided to enable the implementation of the algorithm and software development. Validation studies for each of the derived parameters is included thereby exhibiting the algorithm's ability to meet GOES-R performance specification.

1 INTRODUCTION

1.1 Purpose of This Document

This Algorithm Theoretical Basis Document (ATBD) provides a high-level description of the physical basis for the inference of nighttime water/ice cloud optical depth (COD) and Particle Size (CPS) from imagery taken by the Advanced Baseline Imager (ABI). The ABI will be flown on the GOES-R series of NOAA geostationary meteorological satellites. The COD and CPS will be inferred for all nighttime pixels identified as containing cloud by the GOES ABI cloud type, and for which cloud temperature has been obtained. The COD and CPS are used subsequently to calculate liquid water path (LWP) and ice water path (IWP). All of these parameters can be inter-compared with those derived from active measurements from space-born instruments such as CloudSAT and CALIPSO, as well as ground-based sensors such as microwave radiometers.

1.2 Who Should Use This Document

The intended users of this document are those interested in understanding the physical basis of the algorithms and how to use the output of this algorithm to study or assimilate cloud properties. This document also provides information useful to anyone maintaining or modifying the original algorithm.

1.3 Inside Each Section

This document is broken down into the following main sections.

- **Observing System Overview**: Provides relevant details of the ABI.
- **Algorithm Description**: Provides all the detailed description of the algorithm including its physical basis, the mathematical elements, its input and its output.
- **Test Data Sets and Outputs**: Provides examples of algorithm input and output and describes validation efforts.
- **Practical Considerations**: Provides an overview of the processing considerations for the algorithm.
- **Assumptions and Limitations**: Provides an overview of the current limitations of the approach and provides the plan for overcoming these limitations with further algorithm development.

1.4 Related Documents

This document currently does not relate to any other document outside of the specifications of the current GOES-R Function and Performance Specification (F&PS) and to the references given through out.

1.5 Revision History

Version 2.0 of this document was created by Patrick Minnis of NASA Langley Research Center, Patrick Heck of CIMSS at University of Wisconsin-Madison and colleagues. The intent is for this document to accompany the delivery of version 5.0 of the algorithm to the GOES-R AWG Algorithm Integration Team (AIT). Version 5.0 of the algorithm replaces algorithm Version 4.0 while the ATBD replaces ATBD Version 1.0

2 OBSERVING SYSTEM OVERVIEW

This section describes the products generated by the ABI algorithm for deriving COD, CPS, LWP and/or IWP at night and the requirements it places on the sensor.

2.1 Products Generated

This algorithm is responsible for the calculation of water/ice COD, CPS and water/ice path for all ABI nighttime cloudy pixels. In our context, the determination of nighttime is defined to be where the solar zenith angle for a given pixel is greater than or equal to 90^o. In addition, these same cloud properties are calculated for solar zenith angles greater than or equal to 82^o and less than 90^o, but only in a qualitative sense. Another point to keep in mind is that the current algorithm design utilizes cloud phase (inferred from ABI cloud type) and cloud top temperature. Cloud types and cloud top temperatures are determined by ABI algorithms that must be invoked prior to running the algorithm. An attempt will be made to derive COD, CPS, LWP and/or IWP for all pixels that are cloudy with quality flags indicating the degree of success.

The performance of the algorithm will be sensitive to such issues as sensor or imagery artifacts, instrument noise and imperfections in the knowledge of the sensor response functions. Calibrated observations are critical because the technique utilizes the observed values in conjunction with calculations from a radiative transfer model where accurate radiances are assumed. The channel specifications are given in the current F&PS with pertinent descriptors extracted below in Table 1. These measurement ranges, accuracies and precisions apply to the CONUS, full disk and mesoscale Product Geographical Ranges.

In Table 1 the current F&PS requirements are in black while the F&PS requirements that are awaiting approval by the GSP are given in red. This ATBD assumes that the pending requirements will be approved, so our validation studies were performed with that in mind.

Table 1. Key F&PS product requirements for NCOMP.

Observational Requirement	LEVEL[1]	Geographic Coverage[2]	Horiz. Res.	Mapping Accuracy	Msmnt. Range (liquid / ice)	Msmnt. Accuracy (liquid / ice)	Msmnt. Precision (K)	Refresh Rate	Extent Qualifier[3]
Cloud Optical Depth	T	C	2 km	1 km	1-8	20% 30%	max of 0.5 or 20%	15 min	SZA <65
Cloud Optical Depth	T	FD	4 km	2 km	1-8	20% 30%	max of 0.5 or 20%	15 min	SZA <65
Cloud Particle Size	CT	C	2 km	1 km	2-32 µm 2-50 µm	4µm 10µm	2µm 4µm	5 min	SZA <65
Cloud Particle Size	CT	FD	2 km	1 km	2-32 µm 2-50 µm	4µm 10µm	2µm 4µm	15 min	SZA <65
Cloud Particle Size	CT	M	2 km	1 km	2-32 µm 2-50 µm	4µm 10µm	2µm 4µm	5 min	SZA <65
Liquid Water Path	T	C	2 km	1 km	25-150 g/m2	Greater of 25 g/m^2 or 15%	Greater of 25 g/m^2 or 40%	5 min	SZA <65
Liquid Water Path	T	FD	2 km	1 km	25-150 g/m2	Greater of 25 g/m^2 or 15%	Greater of 25 g/m^2 or 40%	30 min	SZA <65
Liquid Water Path	T	M	2 km	1 km	25-150 g/m2	Greater of 25 g/m^2 or 15%	Greater of 25 g/m^2 or 40%	5 min	SZA <65
Ice Water Path	T	C	2 km	1 km	25-300 g/m2	Greater of 25 g/m^2 or 30%	Greater of 25 g/m^2 or 40%	5 min	SZA <65
Ice Water Path	T	FD	2 km	1 km	25-300 g/m2	Greater of 25 g/m^2 or 30%	Greater of 25 g/m^2 or 40%	15 min	SZA <65
Ice Water Path	T	M	2 km	1 km	25-300 g/m2	Greater of 25 g/m^2 or 30%	Greater of 25 g/m^2 or 40%	5 min	SZA <65

1-T – total column, CT- cloud top, 2-C-Conus, FD- Full disk, M – Mesoscale, 3- SZA- solar zenith angle qualifier

2.2 Instrument Characteristics

Table 2 summarizes the ABI channels used in the algorithm that determines the nighttime cloud optical and microphysical properties. The final channel set may vary as the algorithm continues to mature, but for the 100% version of the code and this ATBD the channels are as indicated. This version of the algorithm uses channels 7, 14 and 15, whereas a future version could also use channels 11 and 16.

Table 2. Channel numbers and wavelengths for the ABI. ✓ indicates usage in current algorithm while # indicates possible future use.

Channel Number	*Wavelength (μm)*	*Used in Algorithm*
1	0.47	
2	0.64	
3	0.86	
4	1.38	
5	1.61	
6	2.26	
7	3.9	✓
8	6.15	
9	7.0	
10	7.4	
11	8.5	#
12	9.7	
13	10.35	
14	11.2	✓
15	12.3	✓
16	13.3	#

3 ALGORITHM DESCRIPTION

Below is complete description of the algorithm at its current level of maturity.

3.1 Algorithm Overview

The COD (τ) and CPS (r_e) are critical for determining the liquid and ice water content of clouds, which impact numerical weather and climate models, as well as any calculations of heating rates and radiative fluxes. The ABI approach for inferring nighttime COD, CPS, LWP and IWP is based on a heritage algorithm from NASA Langley Research Center (Minnis et al. 1995, 2009) that is being used to derive nighttime cloud properties from MODIS imagery for the CERES project, GOES, AVHRR and MTSAT imagery, as well as from other narrowband radiometers aboard other satellites and for a variety of other projects.

The current algorithm, from this point forward referred to as the Nighttime Cloud Optical and Microphysical Properties (NCOMP) algorithm, will use ABI channels 7, 14 and 15. It is anticipated that a future version might also use channels 11 and 16, but this ATBD will refer only to the current version.

3.2 Processing Outline

The processing outline of the NCOMP retrieval algorithm is summarized in Figure 1. The current NCOMP algorithm has been implemented in both online and offline frameworks, at CIMSS and by the AIT, respectively. For development purposes, the offline framework's routines are used to provide all of the observations and ancillary data, although the usage of other frameworks is possible assuming all inputs and ancillary data are supplied. The NCOMP algorithm can run on segments of data, as all algorithms in the offline framework do, but can also run on individual pixels if all of the input data and ancillary data sets are available. A segment is comprised of multiple scan lines.

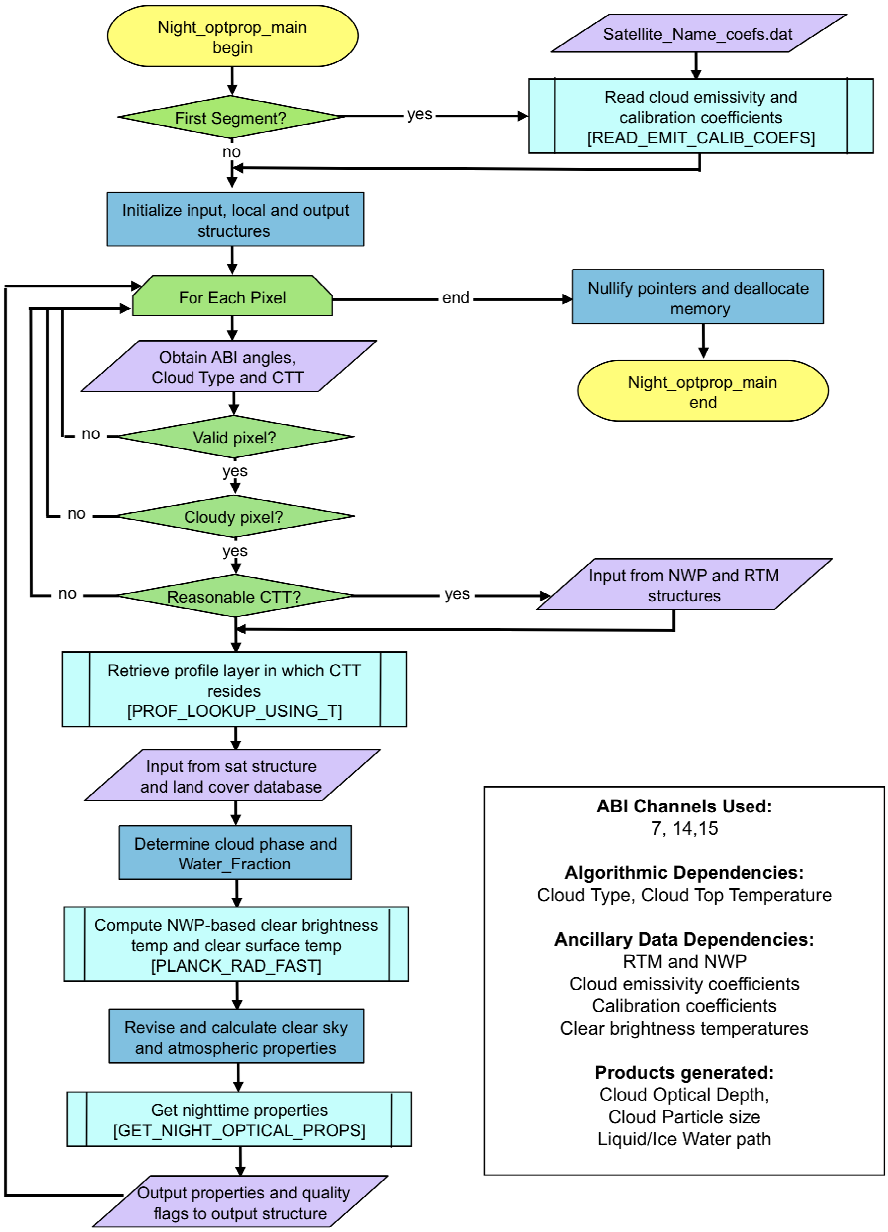

Figure 1. High level flowchart of the Nighttime Cloud Optical and Microphysical Properties algorithm illustrating the main processing sections

3.3 Algorithm Input

This section describes the input needed to invoke and process ABI data with the NCOMP algorithm.

3.3.1 Primary Sensor Data

The list below contains the primary sensor data used by the NCOMP algorithm. By primary sensor data, we mean information that is derived solely from the ABI observations and geo-location information.

- Calibrated radiance for channels 7, 14, and 15
- Calibrated brightness temperature for channels 7, 14, and 15
- Local zenith angle
- Solar zenith angle

3.3.2 Ancillary Data

The following briefly describes the ancillary data required to run the software to infer nighttime COD and CPS and subsequently determine LWP/IWP using the NCOMP algorithm. By ancillary data, we mean data that requires information not included in the ABI observations or geo-location data.

- **Land mask / Surface type**
  A global land cover classification collection created by The University of Maryland Department of Geography (Hansen et al. 1998). Imagery from the AVHRR satellites acquired between 1981 and 1994 were used to distinguish fourteen land cover classes (http://glcf.umiacs.umd.edu/data/landcover/). This product is available at 1 km pixel resolution.

- **Surface emissivity of channels 7, 14 and 15.**
  A global database of monthly infrared land surface emissivity derived using input from the Moderate Resolution Imaging Spectroradiometer (MODIS) operational land surface emissivity product (MOD11). Emissivity is available globally at ten wavelengths (3.6, 4.3, 5.0, 5.8, 7.6, 8.3, 9.3, 10.8, 12.1, and 14.3 microns) with 0.05 degree spatial resolution (Seemann et al. 2007). The monthly emissivities have been integrated over the ABI spectral response functions to match the ABI channels.

- **Clear-sky infrared radiative transfer model calculations**
  Clear-sky top-of-atmosphere (TOA) radiances and brightness temperatures computed for channels 7, 14 and 15. Profiles of clear-sky transmission and radiance are required for the same channels, as well as the surface temperatures. Currently, these clear-sky temperatures and radiances, as well as the radiance and transmission profiles, are obtained by using a fast clear-sky Radiative Transfer

Model (RTM), the Pressure-layer Fast algorithm for Atmospheric Transmisstance (PFAST) with 101 vertical levels that match the temperature profiles described below in the All-sky Temperature profile explanation.

- **All-sky Temperature profiles**
  Knowledge of the atmospheric temperature profiles is required in order to place cloud temperatures at the appropriate level. Currently, these profiles are from GFS, the Numerical Weather Prediction (NWP) data sets available in the offline framework. These profiles are temporally interpolated from 6- or 12-hour model data, horizontally interpolated to either 0.5° or 1.0° grids and vertically interpolated to 101 levels. The details of this data set are contained in the XXXXXX (don't know what the document that contains this info is called).

- **Calibration Coefficients**
  Due to lack of accurate calibration in some SEVIRI channels and the possibility that some ABI channels will need refined calibration during NCOMP processing, the capability to read and utilize instrument-specific calibration coefficients is included. In the 100% delivery only SEVIRI channel-7 brightness temperatures require recalibration, so in that circumstance a calibration is applied. Future versions can have similar calibration procedures for additional channels, but only SEVIRI currently has active recalibration as it is the ABI proxy dataset. A simple slope and offset formulation is used and the file contains a description of the calibration source. These coefficients are read from the same text file as the cloud emittance parameterization coefficients because those are also instrument-specific.

- **Cloud Emittance Parameterization Coefficients**
  The retrieval uses a set of coefficients that allows the invocation of a parameterization that computes cloud effective emittances for a set of 16 cloud particle size models, both water and ice, as a function of local zenith angle, clear-sky temperature, and cloud temperature for each of the 3 ABI channels currently used (Minnis et al. 1998). These parameterizations, detailed in 3.4.2.1, have been calculated for a fixed set of 8 cloud optical depth bins and the resultant cloud emittances are used in the algorithm for computing cloud temperatures in channels 7, 14 and 15 for each pixel. For a given channel, COD bin and CPS model, 30 coefficients are contained in the file, hence the file contains 240 coefficients per channel for each of the 7 water droplet and 9 ice crystal models, i.e., 3840 coefficients per channel. The coefficients are in theory instrument-specific, but the same set of coefficients can usually be used for instruments with similar spectral responses in a given channel. These coefficients are read from the same text file as the calibration coefficients because those are also instrument-specific

3.3.3 Derived Data

The following briefly describes the products from other ABI algorithms that the NCOMP algorithm uses as input. These data are necessary in order to run the software that calculates COD, CPS, LWP and IWP. These data are required information that is not included in the ABI observations or geo-location data.

- **Cloud Type**
  As described in the ABI Cloud Phase/Type ATBD, cloud type and phase are derived prior to the invocation of the NCOMP algorithm. Currently, rather than using the ABI Cloud Phase, the values for ABI Cloud Type are input to the NCOMP algorithm where phase is then determined internally by combining various cloud types. The ABI phase product is determined in a similar manner, but the NCOMP algorithm is currently using its own internal combination scheme. Neither the ABI cloud phase or cloud mask products are being used directly because ABI cloud type results provide additional information and retain flexibility for future enhancements of NCOMP. NCOMP results are not impacted by this internal combination scheme; it serves only to facilitate potential future enhancements. In addition, the internally produced cloud phase allows for processing flags to be set if NCOMP or the ABI Cloud Type product provides an indication that the phase might be ambiguous, e.g., for mixed, multi-layered or super-cooled cloud types. This will enhance validation studies.

- **Cloud Top Temperature**
  As described in the ABI Cloud Temperature/Height ATBD, cloud top temperature is derived prior to the invocation of the NCOMP algorithm.

3.4 Theoretical Description

Knowledge of the LWP and IWP for water and ice clouds, respectively, is one of the primary needs of climate and weather modelers to determine radiation budgets, develop radiative transfer techniques, and modify cloud models and parameterizations. LWP and IWP are not directly retrieved on large spatial scales given current satellite technology, but fortunately, the relatively simple relationships between COD and CPS and the liquid or ice water path allow for their calculation.

The GOES-R Clouds Algorithm Working Group is using a suite of algorithms for daytime and nighttime data, exploiting the strengths of each technique in order to maximize accuracies and provide feedback opportunities between techniques that were independently developed. For NCOMP a heritage algorithm from NASA Langley, the Shortwave-infrared Infrared Split-window Technique (SIST) of Minnis et al (1995, 2009), has been chosen as it is currently being applied to a variety of satellite instruments. SIST is also one of the more robust existing algorithms because it

simultaneously determines phase and cloud temperature/height as well as cloud optical and microphysical properties. The NCOMP algorithm uses differences in cloud brightness temperature, clear-sky temperature, and spectral differences to ascertain both COD and CPS and, in turn, to calculate the LWP and IWP. For the purposes of GOES-R, SIST has been adapted so that it accepts as input the cloud top temperature and cloud type that are determined in other GOES-R algorithms and then calculates both COD and CPS based on those inputs.

3.4.1 Physics of the Problem

Numerous techniques have been developed to retrieve cloud optical and microphysical properties from narrowband radiometer measurements onboard satellites. Many of these techniques exploit spectral differences in visible wavelengths, or wavelengths comprised of both reflected and emitted components, and, therefore, are not applicable to nighttime situations.

3.4.1.1 Thermal Radiative Transfer

A simple radiative transfer relationship that describes an emitted radiance observed by a satellite at a particular wavelength, λ, at temperature T_λ can be expressed as

$$B_\lambda\left(T_\lambda\right) = t_{\lambda u}\left\{t_{\lambda l}\left[1-\varepsilon_\lambda\left(\mu,\tau_\lambda\right)\right]\left[(1-\varepsilon_{s\lambda})\left(L_{\lambda\downarrow s}\right)+\varepsilon_{s\lambda}B_\lambda\left(T_s\right)\right]+\varepsilon_\lambda\left(\mu,\tau_\lambda\right)B\left(T_{cld}\right)\right\} \quad (1)$$

where B_λ is the Planck function, T_S is the surface temperature, T_{cld} is the cloud temperature, $L_{\lambda\downarrow s}$ is the downwelling radiance at the surface, $\varepsilon_{s\lambda}$ is the surface emittance, $\varepsilon_\lambda(\mu,\tau_\lambda)$ is the effective cloud emittance at cosine local zenith angle μ and cloud optical depth of τ. The transmission and effective emission of the atmosphere above and below the cloud is represented by $t_{\lambda u}$ and $t_{\lambda l}$, respectively. If scattering is neglected, then

$$\varepsilon_\lambda = 1-\exp\left(-\tau_{a\lambda}/\mu\right) \quad (2)$$

where the cloud absorption optical depth $\tau_{a\lambda} = (1 - \tilde{\omega}_o)\tau_\lambda$ and $\tilde{\omega}_o$ is the single scattering albedo. For semi-transparent clouds, it is possible to estimate ε_λ and T_{cld} from simultaneous measurements at two different wavelengths λ_i and λ_j, if the clear-sky temperature at that wavelength, $T_{cs\lambda}$, and the relationship between $\varepsilon_{\lambda i}$ and $\varepsilon_{\lambda j}$ is known and $\varepsilon_{\lambda i} \neq \varepsilon_{\lambda j}$. If ε_λ is known, then τ_λ can be determined from the equation above or some other function that relates the two quantities. In GOES-R applications, T_{cld} is known from other GOES-R algorithms so it is theoretically possible to determine particle size, r_e, and τ_λ, assuming that the optical properties of the clouds are different at wavelengths λ_i and λ_j. As discussed below, many techniques make use of the brightness temperature

difference BTD_{i-j} between T_i and T_j to provide information about the particle size and optical depth (Note that for consistency with the published literature cloud particle size is sometimes referred to as effective radius in this ATBD).

3.4.1.2 Cloud Microphysics

Over some distance, z_1 to z_2, the spectral optical depth for a given size distribution can be determined from

$$\tau_\lambda = \pi Q_e \int_{z_1}^{z_2} N r_e^2 dz \qquad (3)$$

where Q_e is the extinction efficiency and N is the total particle number density. For a water cloud, the particle size between some size distribution between r_1 and r_2 is

$$r_e = \frac{\int_{r_1}^{r_2} r \pi r^2 n(r) dr}{\int_{r_1}^{r_2} \pi r^2 n(r) dr} \qquad (4)$$

where $n(r)$ is the number density of droplets with radius r. For ice particles, using the techniques from Minnis et al. (1995) the effective diameter is

$$D_e = \frac{\int_{L_1}^{L_2} D(L) \pi A_e(L) n(L) dL}{\int_{L_1}^{L_2} \pi A_e(L) n(L) dL} \qquad (5)$$

where $D(L)$ is the volume equivalent diameter of the hexagonal ice crystal of length L and width d. A_e is the cross-sectional area where there is an assumed monotonic relationship between L and d for the hexagonal ice columns as defined in Takano and Liou (1989). The equivalent particle size can be computed from D_e using the following equation,

$$r_e = 0.4441\ D_e + 1.0013\text{E-}3\ D_e^2 + 7.918\text{E-}9\ D_e^3 \qquad (6)$$

where D_e has been defined for the particle size distributions given by Minnis et al. (1998). The LWP or IWP is computed as a function of τ and r_e as explained in section 3.4.2.2.

Thermal-only techniques that are applicable during either day or night are typically based on BTDs between two or more thermal channels, e.g., Inoue (1985), Ackerman et al. (1990), Lin and Coakley (1993), Baum et al. (1994), Minnis et al. (1995, 2009), Fu and Sun (2001), Katagiri and Nakajima (2004), and Chiriaco et al. (2004). While each of these algorithms and their variations are capable of deriving COD and CPS, some also simultaneously determine cloud temperature, height and other interdependent quantities,

but most assume a priori knowledge of either the cloud height and/or thermodynamic phase.

These methods ultimately rely on the differences in the imaginary indices of refraction (IIR) among the various channels. Figure 2 plots the IIRs for liquid and ice water from Downing and Williams (1975) and Warren (1984) for part of the relevant spectral range. Both the 11- and 12-µm channel ice IIRs are twice their respective water values. However, the difference between the 11- and 12-µm ice IIRs is double the difference between their water counterparts. For the 8.5-µm channel, the IIRs are the same for ice and water, while the ice and water IIRs for the 3.9-µm channel (not shown) are roughly 5% of the values for the 11-µm channel. These differences in IIR among the

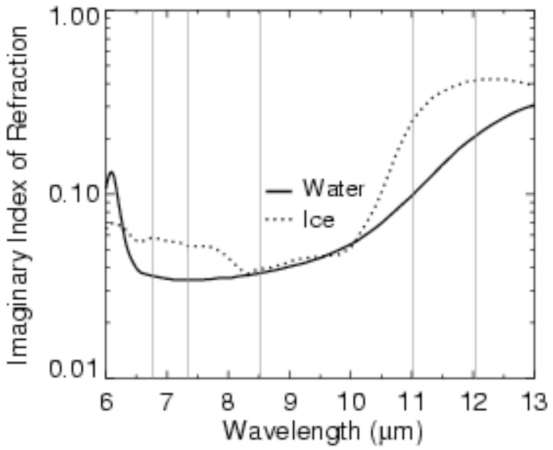

Figure 2. Imaginary indices of refraction for part of the infrared spectrum.

channels translate to differences in absorption as represented by the single scattering albedo computed via Mie scattering theory for water droplets or, for ice crystals, via geometric optics or some other technique. As radius increases, both the path length through the particle and $\tilde{\omega}_o$ increase for strongly absorbing wavelengths such as those in Fig. 2. For weakly absorbing wavelengths (e.g., 3.9 µm), $\tilde{\omega}_o$ decreases with increasing radius (e.g., Minnis et al., 1998). For both absorption types, $\tilde{\omega}_o$ approaches 0.5 because the diffraction takes out about half of the energy available for absorption. Because of these spectral absorption differences, the BTD between a given pair of channels will depend on the particle size, optical depth, and difference between the surface and cloud temperatures.

The reference wavelength for most cloud retrievals is the 0.64-µm or VIS channel. The spectral optical depth is related to the VIS optical depth through the extinction efficiencies,

$$\tau_\lambda = \tau_{VIS}\, Q_\lambda / Q_{VIS}. \qquad (7)$$

For smaller particles, Q_λ ranges from 0.3 to 1.9 at longer wavelengths. For larger particles Q_λ varies from 1.9 to 2.2, while it is typically between 2.0 and 2.6 for 3.9 and the VIS wavelengths (e.g., Minnis et al., 1998). Given (2) and (7), the emittances for larger particles are ~0.95 and 0.982 for τ_{VIS} = 6 and 8, respectively, at a nadir view for both 11 and 12 μm. Thus, the $BTD_{11\text{-}12}$ approach zero for optical depths τ_{VIS} > ~6. Since most geostationary satellite observations are taken off nadir, the limiting optical depths will typically be much smaller (~3 for μ = 0.5). For smaller particles, the limiting optical depths can be somewhat smaller. Thus, the SIST-type retrievals are constrained mostly to semi-transparent clouds. This limits the amount of information that can be retrieved compared to daytime when the use of solar reflectance yields optical depths exceeding 100.

The theoretical curves in Figure 3, reproduced from Minnis et al. (1998) show the typical behavior of the BTDs as functions of particle size and phase for a cloud temperature of 260 K for AVHRR channels, but the situation is analogous for SEVIRI and ABI channels. That is, $BTD_{3.75\text{-}10.8}$ tends to decrease with increasing particle size for ice clouds (Fig. 3a) and vice versa for water clouds (Fig. 3b). However, $BTD_{11\text{-}12}$ decreases with increasing particle size for both water and ice (Figs. 3c,d). The BTD values are also dependent on the difference between T_{cld} and T_{cs} because they constrain the maximum

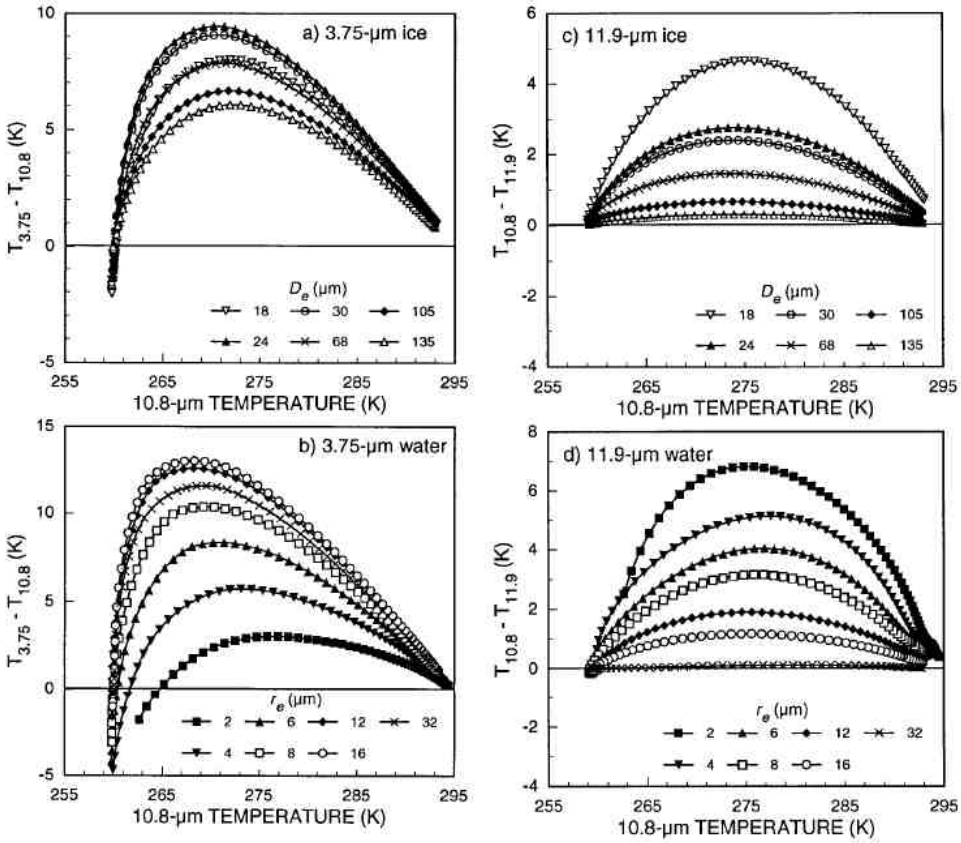

Figure 3. Modeled BTDs from the emittance parameterizations for clouds of various r_e and D_e for T_{cs} = 295, T_{cld} = 260 K, τ = 16 and local zenith angle = 30°.

values. Thus, usable information is available over a greater range of τ_{VIS} for a greater contrast between the surface and cloud temperatures. As T_{cld} approaches T_{cs}, the utility of the SIST diminishes, but not entirely since $BTD_{3.75\text{-}10.8}$ tends toward some negative limiting value because of scattering at 3.75 µm.

Discussion of the particle size limits that can be retrieved using these techniques can be found in Lin and Coakley (1993).

3.4.2 Mathematical Description

NCOMP determines the cloud optical depth and cloud particle size that produce modeled brightness temperatures that are closest to the observed brightness temperatures for each ABI proxy pixel. Observed BTDs are compared to modeled, i.e, simulated, BTDs and cloud physical parameters are inverted. The effective radius, r_e, and τ that produce the minimum difference between observed and modeled BTDs for each pixel are assumed to describe the cloud. The phase-appropriate water path, either LWP or IWP, is calculated based on the retrieved r_e and τ.

3.4.2.1 Emittance Parameterizations

Similar to the methods of Minnis et al. (1998), the cloud emittance models used by NCOMP comprise a set of coefficients that were calculated for the GOES 3.9-, 10.8- and 12-µm channels. While the GOES channel characteristics vary from the analogous ABI channels (7, 14 and 15), the quality of the retrieved parameters is thought to be sufficient for the purposes of testing NCOMP using SEVIRI data. The effective emittance, which includes the effects of both scattering and absorption, is used instead of the absorption emittance to maximize the accuracy of the simulated radiances. For each set of water droplet and ice crystal models and for the aforementioned wavelengths, the following regression formula was fitted to effective emittances computed using radiances calculated with the adding-doubling radiative transfer model of Minnis et al. (1993):

$$\varepsilon_\lambda(\zeta,\mu,\xi) = \sum_{i=0}^{2}\sum_{j=0}^{4}\sum_{k=0}^{1} d_{ijk}\zeta^i\mu^j\xi^k \qquad (8)$$

where $\zeta = 1/\ln(\Delta T_{sc})$, $\Delta T_{sc} = T_{cs} - T_{cld}$, and $\xi = 1/\ln(T_{cs})$. The clear sky temperature, T_{cs}, is equivalent to $\varepsilon_{s\lambda}B_\lambda(T_s)$ in the thermal radiative transfer equation and includes atmospheric attenuation because it is a TOA quantity, i.e., T_{cs} is the upwelling brightness temperature at the bottom of the cloud. A set of coefficients, d_{ijk}, was determined for each optical depth node and particle size model, ice and water, where i, j, and k are the exponents for ζ, μ and ξ, respectively. These coefficients and the order of the exponents were determined by minimizing the squared error in the regression analyses, which generated nine sets of 30 coefficients for each microphysical model and spectral band. The complexity of (8), as compared to (2), is necessary because (2) cannot account for scattering by the cloud particles. The parameterizations were developed for 7 water

droplet models using Mie scattering theory and 9 ice crystal size distributions using hexagonal columns and ray-tracing to obtain optical properties. The particle size models and their respective cloud particle sizes are detailed in Table 3. The calculations were performed for 8 nodes of visible τ ranging from $\tau = 0.25$ to $\tau = 32$, as well as for realistic ranges of T_{cs} and T_{cld}.

Table 3. Water and ice crystal particle size models used in emittance parameterization.

Effective Radius/Diameter	*Phase*
r_e = 2, 4, 6, 8, 12, 16 and 32 µm	water
D_e = 5.83, 18.15, 23.86, 30.36, 45.30, 67.60, 104.9, 123.0, and 134.9 µm	ice

The mean rms errors of ε_λ from (8) are less than 0.001 and 0.002 for $\lambda = 12$ and 11 µm, respectively, compared to the complete adding-doubling calculations. For $\lambda = 3.9$ µm, the rms errors range from 0.003 for the largest water droplets to 0.02 for the $r_e = 2$ µm, and from < 0.001 for large ice crystals to 0.005 for the $D_e = 5.83$ µm. The parameterized emittances yield uncertainties in simulated brightness temperatures of ~0.05 K for 11- and 12-µm channels and ~0.5 K at 3.9 µm for most conditions. More information about the parameterizations and adding-doubling calculations can be found in Minnis et al. (1998). The parameterizations can be created for other instruments and wavelengths and, if deemed necessary, will be provided by NASA Langley.

3.4.2.2 Retrieval Technique

The NCOMP algorithm utilizes the parameterizations of effective emittance in an iterative scheme that minimizes the BTDs between the computed and observed temperatures at 3.9, 11.2 and 12.3 µm. For each ABI pixel for which a Cloud Type and T_{cld} have been provided, the emittance parameterization is first used to compute $\varepsilon_{11.2}$ for each phase-appropriate particle size model using ΔT as computed from the input T_{cs} and T_{cld}. As described in 3.3.3 and as shown in Table 4, the phase is determined by collapsing the ABI Cloud Type into NCOMP phase categories. In the iteration initialization step for

Table 4. Assignment of cloud phase from ABI Cloud Type in NCOMP.

ABI Cloud Type and Value	*NCOMP Phase*
Clear (0)	no analysis
Fog (1)	water
Water (2)	water
Supercooled (3)	water
Mixed (4)	water
Tice (5)	ice
Cirrus (6)	ice
Overlap (7)	ice
Overshooting (8)	ice
Unknown (9)	no analysis

each particle size model, a first guess determination of $\varepsilon_{11.2}$ is made with τ assumed to be 1.0 and an initial estimate of the modeled brightness temperature, $T'_{11.2}$, is produced using Equation (1) with the appropriate above- and below-cloud atmospheric transmittances from the RTM, as well as T_s and T_{cld}. An iterative scheme then commences by adding 0.1 to τ, computing a new $T'_{11.2}$ and the accompanying differences between the two $T'_{11.2}$ guesses and the observed temperature $T_{11.2}$. After these first two guesses are made, the scheme iterates in τ by continuously updating τ weighted by the ratio of the τ differences to the corresponding temperature differences, hence for each iteration, m, the subsequent guess τ_{m} is

$$\tau_{m} = \tau_{m-1} + (T'_{11.2,m} - T_{11.2})(\tau_{m-1} - \tau_{m-2}) / [(T'_{11.2,m} - T_{11.2}) - (T'_{11.2,m-1} - T_{11.2})]. \quad (9)$$

The iteration continues either for a maximum of 15 steps or until the difference in subsequent τ calculations is 0.10, whichever occurs first. At this point each τ has been determined for each cloud particle size model as this procedure has been invoked for each of the 7 water or 9 ice models.

Note that in the above scheme whenever $\varepsilon_{11.2}$ is needed when calculating $T'_{11.2}$ for a particular combination of T_s, T_{cld}, $T_{11.2}$, τ and r_e for a cloud particle size model, it is necessary to interpolate between the optical depth nodes of the emittance parameterization. NCOMP utilizes a standard Lagrangian N-point interpolation scheme of emittance on natural log of τ using the parameterization τ nodes of 0.25, 0.5, 1.0, 2.0, 4.0, 8.0, 16.0 and 32.0.

The τ calculated as above for each of the phase-appropriate models is then used to calculate the simulated temperatures for the other two NCOMP channels, $T'_{3.9}$ and $T'_{12.3}$. For both 3.9 and 12.3 μm, the emittance parameterization is invoked again, although for

these channels τ has already been determined so no iteration in τ is needed. At this point then, for each particle size model τ is set as are $T'_{3.9}$, $T'_{11.2}$ and $T'_{12.3}$, each with its appropriate $\varepsilon_{3.9}$, $\varepsilon_{11.2}$ and $\varepsilon_{12.3}$, but these solutions are only for the r_e of the 7 water models if the inferred phase was water or, conversely, the 9 ice models if ice. An error for each of the models

$$E(r_e) = [(T'_{3.9} - T'_{11.2}) - (T_{3.9} - T_{11.2})]^2 + [(T'_{11.2} - T'_{12.3}) - (T_{11.2} - T_{12.3})]^2 \quad (10)$$

is computed from the BTDs in order to determine which model with its corresponding τ and ε best describes the observed brightness temperatures, i.e., has the smallest $E(r_e)$.

Once this minimum error model n with its associated r_e is identified, an interpolation scheme that utilizes the same iterative τ determination method as above is invoked to interpolate between adjacent models and their τ nodes which allows for the computation of off-node τ values and pinpointing of the actual r_e that is likely to lie between adjacent particle size models. Note that for both water and ice, models are always ordered by increasing r_e. First, a model-dependent particle size step is chosen from Table 5 that is used to reduce $r_e(n)$, the r_e for model n, and calculate a new solution between particle size

Table 5. Particle Size steps for interpolating between particle size models.

Model Effective Radius/Diameter	*Phase*	*Particle Size Step*
2 to 16 µm	water	0.10
16 to 32 µm	water	0.20
5.83 to 123.0 µm	ice	0.20
123.0 to 134.9 µm	ice	0.50

models n and $n-1$. The first calculation away from n is for $r_e(n)$ reduced by the step value and a new error is recomputed using Equation (10). The same procedure is repeated between models n and $n+1$ with $r_e(n)$ increased by the step, resulting in the computation of a high side error. It is assumed that the side of model n with the lowest error will contain the ultimate solution, so the two $E(r_e)$ on either side of model n are compared to each other, hence determining the side that contains the solution.

When decreasing r_e from the particle size associated with model n, a new τ is necessarily calculated with each computation of $E(r_e)$, iterating to obtain τ as discussed earlier, but now linearly interpolating between $\varepsilon_{11.2}(n)$ and $\varepsilon_{11.2}(n-1)$ based on the appropriate step (still from Table 5) divided by $r_e(n) - r_e(n-1)$. This weighted $\varepsilon_{11.2}$ is in turn used to compute a weighted $T'_{11.2}$ using Equation (1). Similarly, during each step away from $r_e(n)$ when $T'_{3.9}$ and $T'_{12.3}$ are computed for usage in Equation (10), $\varepsilon_{3.9}$ and $\varepsilon_{12.3}$ use the same linear weighting scheme. Step calculations when increasing r_e use this same process, but the linear interpolation uses the appropriate step divided by $r_e(n+1) - r_e(n)$.

Once it is known which of the low or high sides of model *n* contains the best solution, the technique focuses on the low error side and successively decreases or increases r_e by the same step factor until a minimum $E(r_e)$ is reached. When that minimum is reached, the corresponding τ and r_e are declared the best possible solution.

If the smallest phase-appropriate particle size model is associated with the smallest error, i.e., n=1, then it is not necessary to compute both a low side and high side error. Only the $E(r_e)$ for successive steps increasing from $r_e(n)$ are calculated and a solution is chosen when the error minimizes or when 99% of $r_e(n+1)$ - $r_e(n)$ has been traversed. Likewise, when the largest phase-appropriate model is associated with the smallest error, the $E(r_e)$ for successive steps decreasing from the largest model's particle size are calculated and a solution is chosen when the error minimizes or when 99% of $r_e(n)$ - $r_e(n-1)$ has been traversed.

Because of the need to conduct multiple iterative steps when interpolating between models and model nodes, the emittance parameterization is invoked numerous times reinforcing the need for not including explicit radiative transfer steps in the retrieval scheme.

The phase-appropriate water path, either LWP or IWP, is calculated based on the final values of the retrieved r_e and τ with methods that are similar to those described by Minnis et al. (1998). For water the extinction efficiency, Q_e, is computed from a simple quadratic parameterization in the form

$$Q_e = a_0 + a_1 \ln(r_e) + a_3[\ln(r_e)]^2 \qquad (11)$$

where a_0 = 2.416, a_1 = -0.1854 and a_3 = 0.0209. The LWP is then obtained with

$$LWP = \frac{4}{3Q_e}\tau r_e. \qquad (12)$$

For ice, another parameterization yields

$$IWP = \tau[b_0 D_e + b_1(D_e)^2 + b_3(D_e)^3] \qquad (13)$$

where b_0 = 0.259, b_1 = 0.000819 and b_3 = -0.00000088.

Note that accurate NCOMP retrievals of τ and r_e are not possible for optically thicker clouds, as detailed in 3.4.1.2, and that retrievals for overlapped clouds will be less certain than those for single layer clouds due to the assumption that the observed radiance of a cloudy pixel is emitted from a single-layer cloud. Although the GOES-R NCOMP F&PS requirements apply only for single layer clouds with $1 \leq \text{COD} \leq 5$, NCOMP does provide qualitative retrievals of COD, CPS, LWP and/or IWP for situations when COD is less than or equal to 16. While retrievals in these are not likely to be reliable, we have included them so that further validation studies of these more difficult cases and potential

algorithm enhancements can continue. For NCOMP, if the retrieved COD is greater than 16, then COD is set to 16 and the remaining parameters are retrieved as if COD was equal to16.

The capability to use default particles sizes and optical depths in the case of optically thick clouds, say when COD > 5, is also included, but not utilized in the 100% code delivery. The selection criteria for the default COD and CPS are given by Minnis et al. (2009) with values ranging from τ =8, 16, or 32, r_e = 6, 8, or 10 µm, and D_e = 24 or 64 µm, depending on surface type and cloud temperature. These will be fully discussed should the range of COD of the quantitative retrievals for clouds with $1 \leq \text{COD} \leq 5$ need to be expanded in the future.

As mentioned in 2.1, NCOMP is responsible for calculating COD, CPS, LWP and IWP at night and when 82^o < solar zenith angle and < 90^o, but for the latter in a qualitative sense only. In twilight conditions the same technique as described above is utilized, but at its current level of maturity, only the 11.2- and 12.3-μm ABI channels are used due to the complicating factor of modeling the reflected solar radiation in the 3.9 μm measurements. The computations and logic are all identical, but Equation (10) reduces to

$$E(r_e) = [(T'_{11.2} - T'_{12.3}) - (T_{11.2} - T_{12.3})]^2 \qquad (14)$$

and all calculations related to the 3.9-μm channel are eliminated. NASA Langley does employ the 3-channel technique for twilight angles in its operational and research retrievals, but in the GOES-R framework the additional overhead and coding intricacies attributable to including look-up tables for simulating the reflected portion of the 3.9 µm radiances was judged to be unnecessary for qualitative-only results. Should the GOES-R AIT desire quantitative results during twilight in the future, NASA Langley can provide these items, hence increasing the accuracy of twilight NCOMP retrievals.

3.4.3 Algorithm Output

The output of the NCOMP provides the following ABI cloud products:

- Visible Cloud Optical Depth (dimensionless)
- Cloud Particle Size (μm)
- Liquid Water Path (gm^{-2})
- Ice Water Path (gm^{-2})

All of these products are derived at the pixel level for all cloudy pixels with valid retrievals of cloud type and cloud temperature. The Full Disk Cloud Liquid Water Path product has a Mode 3 30 minute refresh, the Cloud Particle Size Distribution has a Mode 4 Full Disk 15 minute refresh, and the Cloud Optical Depth has a Mode 3 CONUS 15 minute refresh, therefore they should be run once every 30 minutes, 15 minutes and 15 minutes, respectively. To create the Cloud Optical Depth 4 km Full Disk Product, the Cloud Optical Depth good quality pixels will be averaged over a 2 x 2 block of pixels. In

addition, the NCOMP will derive the quality and processing flags as detailed in Tables 6 and 7, respectively, in 5.3.

The output files are in HDF following the examples of all other ABI cloud products.

* note: An ATBD section describing metadata, diagnostic/intermediate information and whether or not the framework output matches the research code's output has been requested for this section. We are not privy to the matching information and do not understand this request, however, we would gladly include it if it is explained further.

4 TEST DATA SETS AND OUTPUTS

4.1 Simulated Input Data Sets

As described below, the proxy data set used to test the NCOMP is comprised of SEVIRI observations. The time periods chosen consisted of a 10-week data set including imagery from August 2006, February 2007, April 2007 and October 2007, thereby accounting for seasonal variations. The analysis spans the entire SEVIRI domain and should therefore encompass a full range of conditions.

4.1.1 SEVIRI Data

SEVIRI provides 11 spectral channels with a spatial resolution of 3 km and a temporal resolution of 15 minutes. SEVIRI currently represents the best source of data for testing and developing the NCOMP. Figure 4 is a full-disk SEVIRI 10.8-µm image from a test case on 0000 UTC on October 1, 2007. The SEVIRI data were provided by the SSEC Data Center.

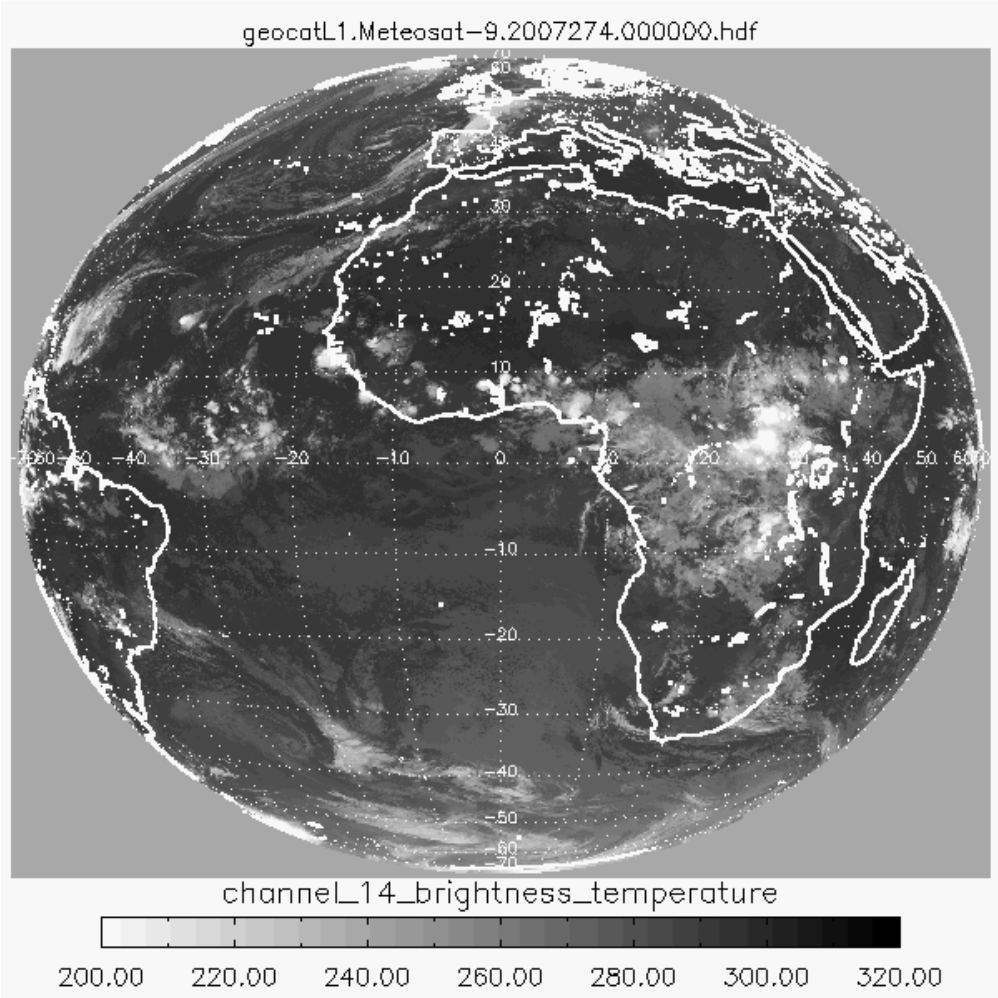

Figure 4. Full disk 10.8-µm grayscale image from SEVIRI for 0000 UTC on 1 October, 2007. It simulates the ABI 11.2-µm channel.

4.1.2 ABI-Derived Inputs

In addition to the image spectral radiances, inputs from other ABI products, in particular, T_{cld} and Cloud Type, are needed to execute NCOMP. Figures 5 and 6 show the values of T_{cld} and Cloud Type, respectively, for the test case of 0000 UTC, 1 October 2007. These ABI-derived products along with the $\varepsilon_{s\lambda}$, and T_s, surface type, and profiles of spectral atmospheric transmissivities and temperatures are then used to compute the modeled top-of-atmospheric brightness temperatures as in Equation (1). The results are then used to solve for r_e and τ. Note that the Cloud Type product is combined internally in NCOMP to produce an NCOMP version of cloud phase, as detailed in 3.3.3 and in Table 4.

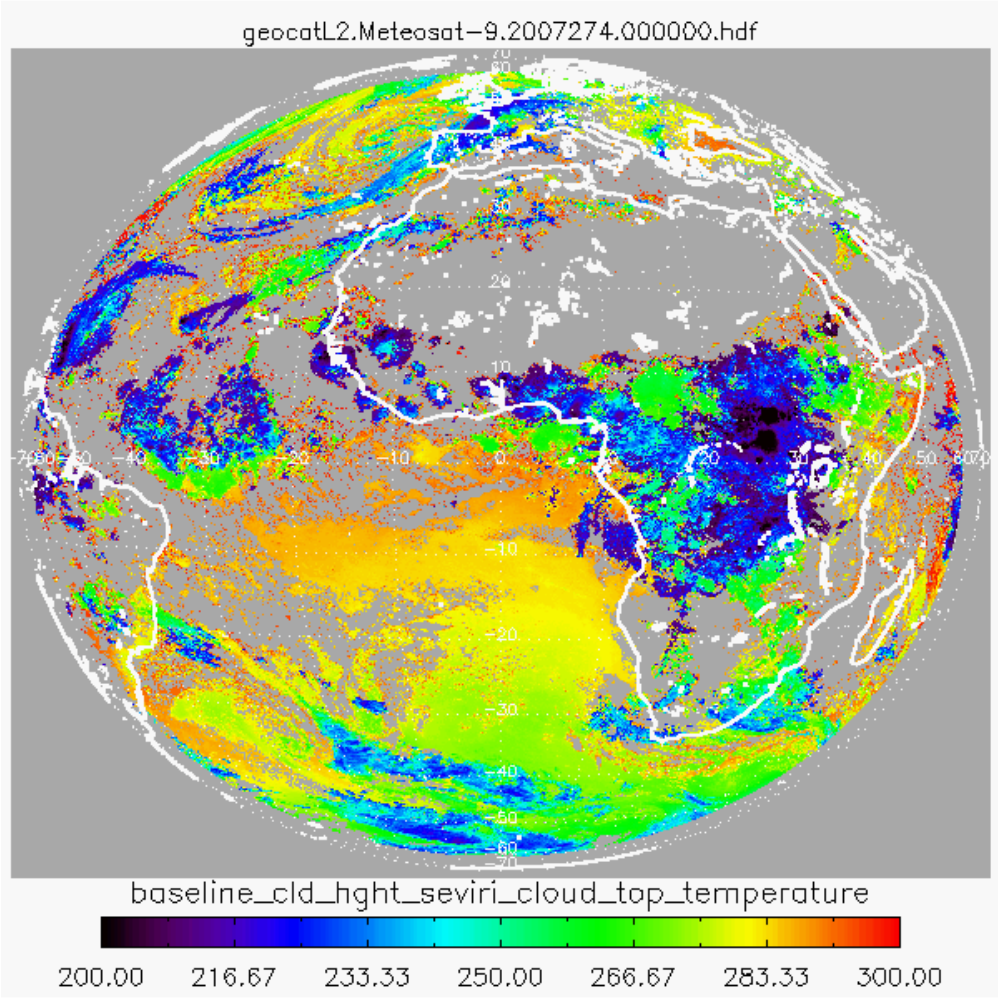

Figure 5. T_{cld} (K) input from ABI Cloud Height/Temperature algorithm for 0000 UTC, 1 October 2007.

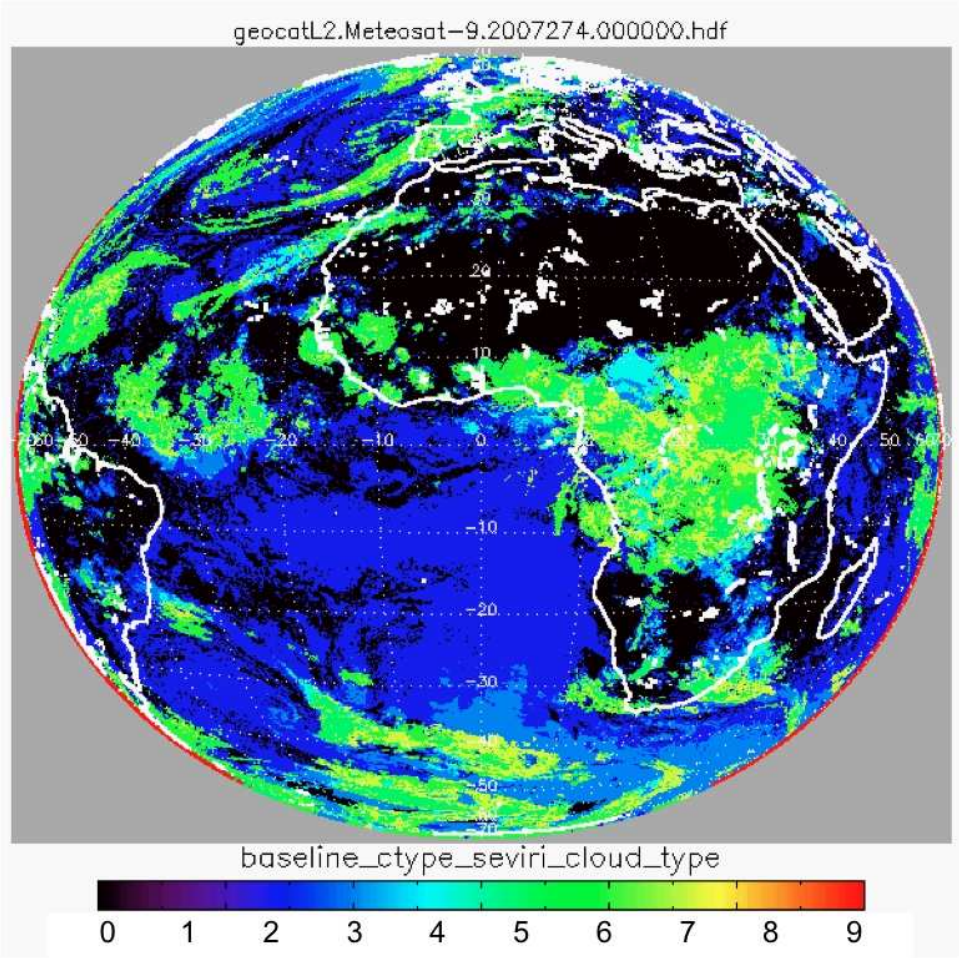

Figure 6. Cloud phase input from ABI Cloud Phase/Type algorithm for 0000 UTC, 1 October 2007. The Cloud Type is collapsed as in Table 4 for usage in NCOMP.

4.2 Output from Simulated Input Data Sets

Preliminary NCOMP products in HDF files were generated using the SEVIRI data for several test cases during the 10-week validation period. Figures 7-10 show the NCOMP output for cloud optical depth, cloud particle size, liquid water path and ice water path. These images correspond to 0000 UTC, 1 October 2007.

The ice cloud optical depths (Fig. 7) in the Southern Hemisphere are mostly less than 6, while a few ice cloud systems over north central Africa have $\tau > 6$ with some values exceeding 16. Liquid and mixed water cloud optical depths are more variable over the image with values ranging from 2 to 16 or more. The radius retrievals appear to be more homogeneous with most r_e(ice) values reaching the plotted particle size models' upper limit of 60.0 μm for ice and many r_e(water) values maximizing at 32 μm. There is, however, more variability in r_e(water) with values between 8 and 16 μm.

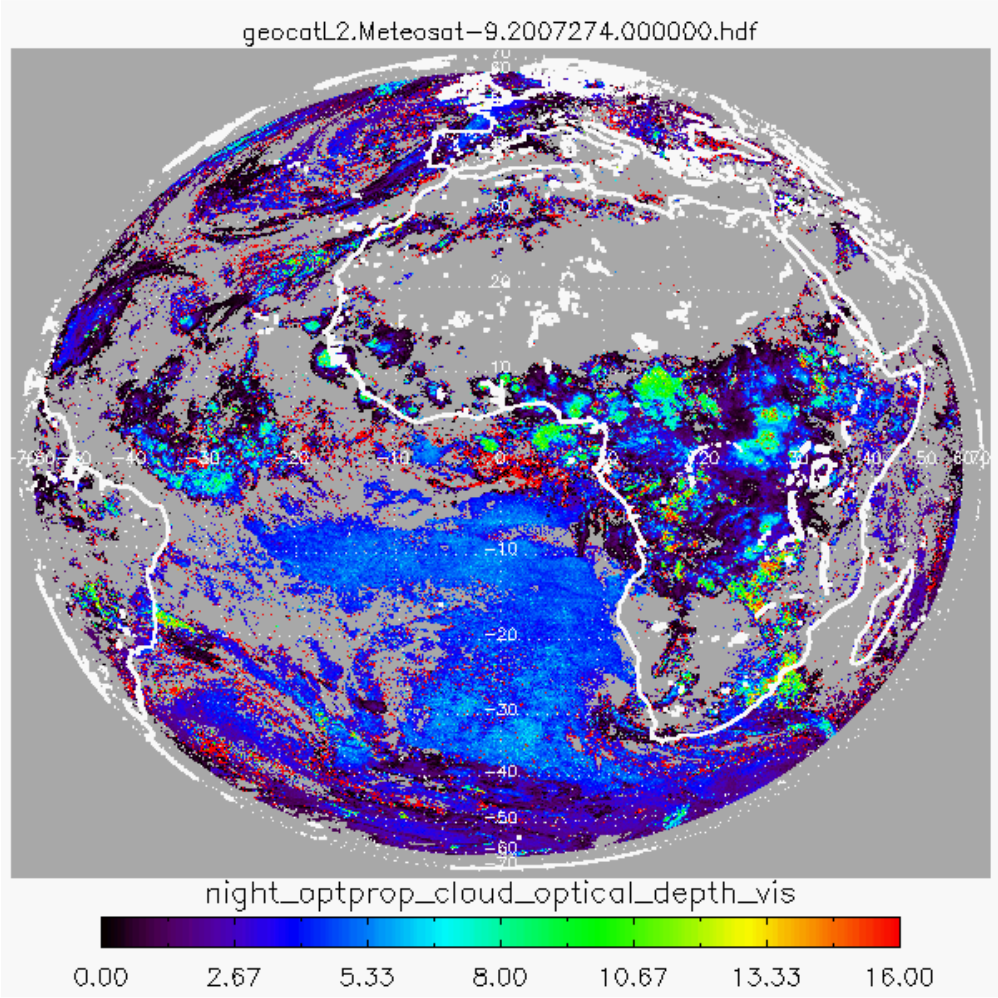

Figure 7. Example of output cloud optical depth from ABI NCOMP algorithm for 0000 UTC, 1 October 2007.

Since most of the retrieved optical depths and particle size values are very small, the resulting LWP values (Fig. 9) are quite small with most values < 40 gm^{-2}. Larger values are found only where the algorithm returned the maximum r_e. In those instances (red in both Figs. 8 and 9) LWP > 100 gm^{-2}. Despite the apparent homogeneity in r_e(ice), the IWP values (Fig. 10) are much more variable, primarily because r_e(ice) is so large. Small changes in τ yield significant changes IWP on the scale shown in Fig. 10.

It is clear from these figures that the NCOMP is producing robust results, but not necessarily at the level expected when compared with SIST. For example, Figure 11 shows the results of applying the SIST, outside of the offline framework, to a Meteosat-9 SEVIRI image (Fig. 11a) taken at 2215 UTC, 17 June 2008. The phase (Fig. 11b) colors are different than those in Fig. 6 with green indicating clear and liquid and ice water shown in blues and red, respectively. The optical depths (Fig. 11c) range from less than 1 for many ice clouds up to 32 for some of the convective clouds. The values of r_e(water)

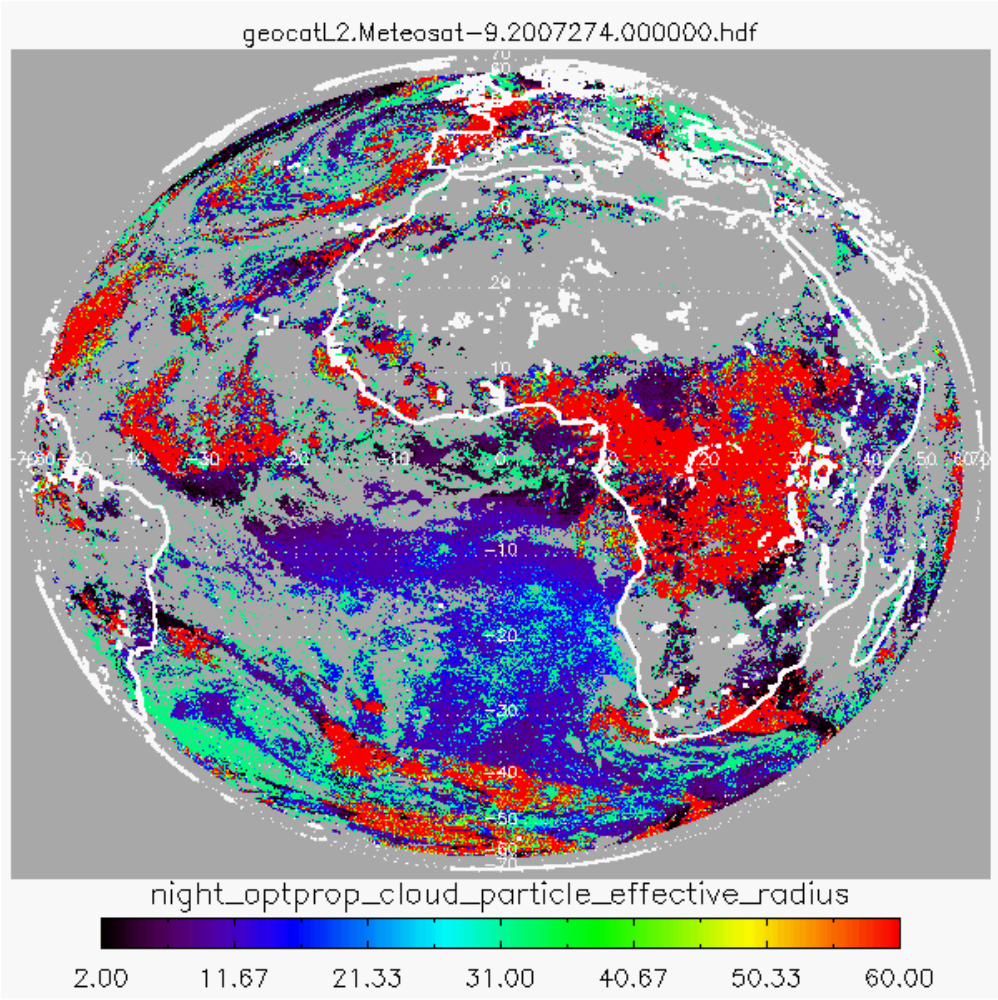

Figure 8. Example of output cloud particle size (μm) from ABI NCOMP algorithm for 0000 UTC on 1 October, 2007.

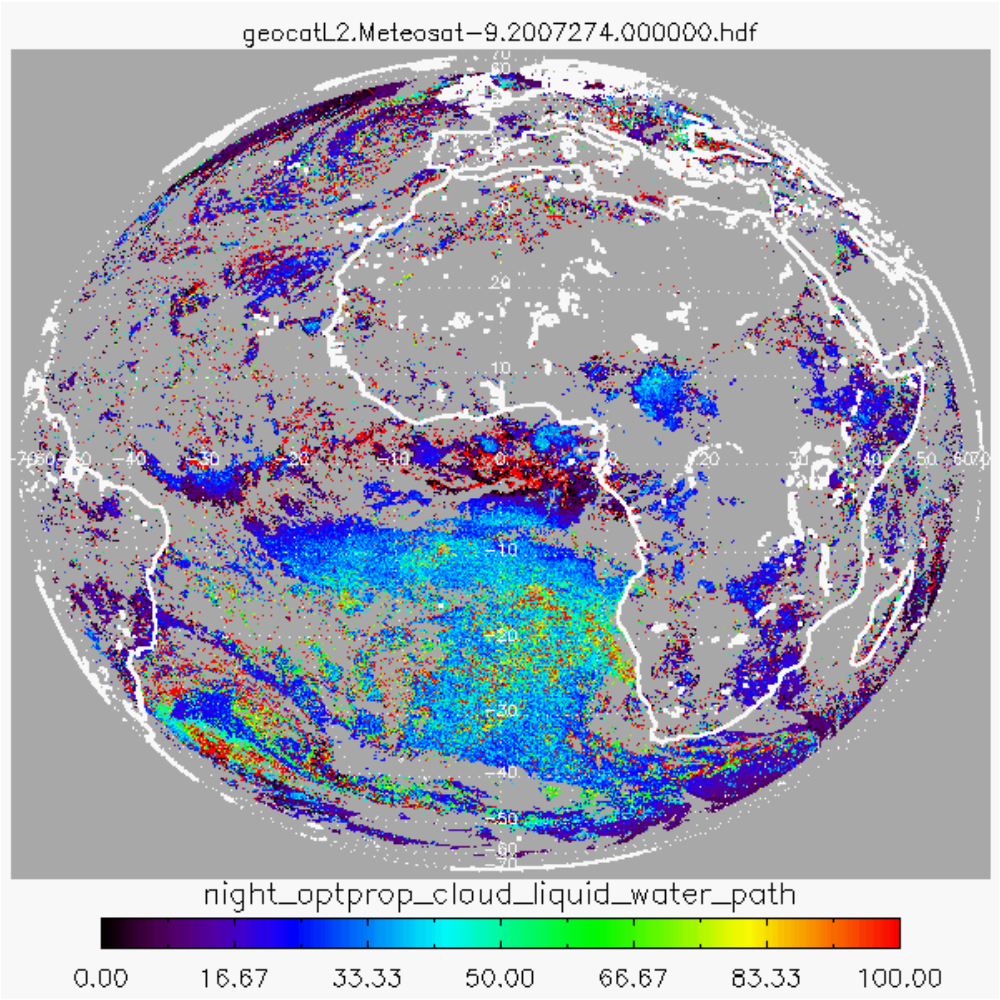

Figure 9. Example of output cloud liquid water path (g m^{-2}) from ABI NCOMP algorithm for 0000 UTC, 1 October 2007.

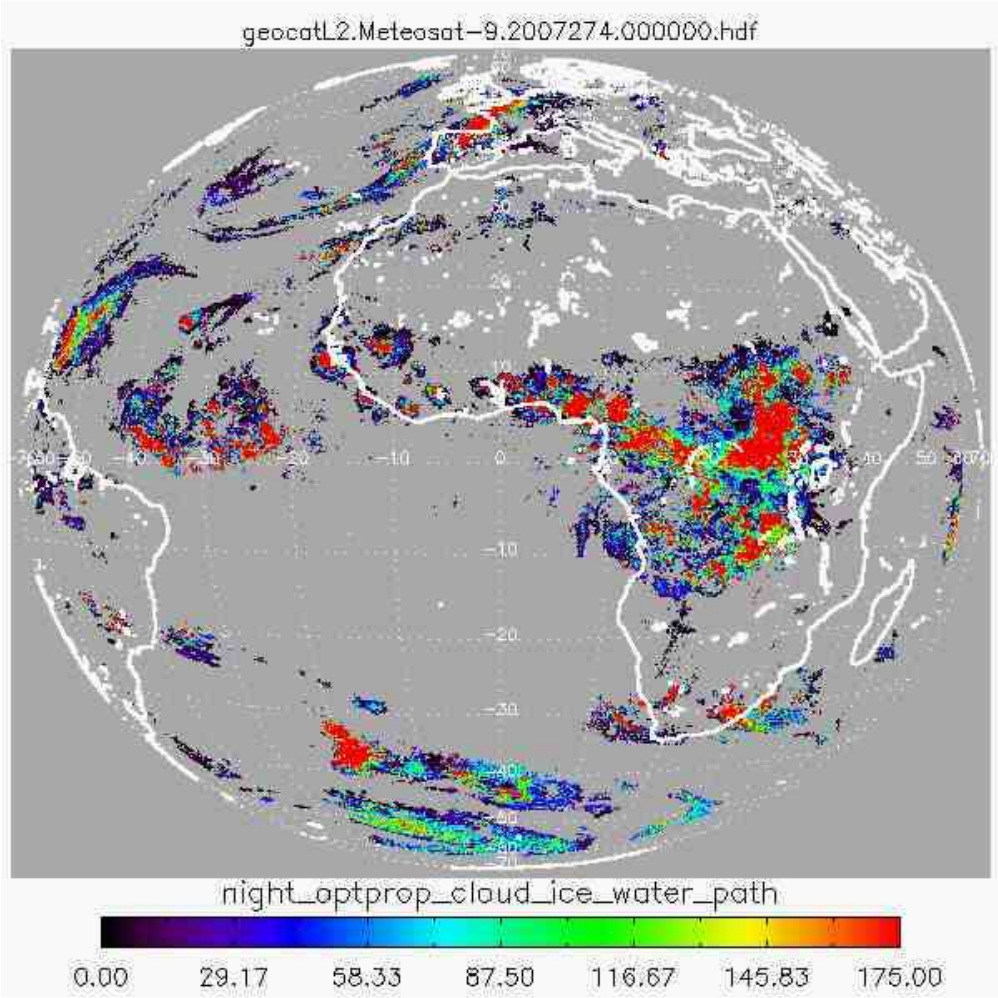

Figure 10. Example of output cloud ice water path (g m^{-2}) from ABI NCOMP algorithm for 0000 UTC, 1 October 2006.

in Fig. 11d range from 6 µm over Brazil to > 25 µm over some of the ocean areas. Values for D_e (Fig. 11e) vary from < 15 µm up to the maximum value. A smaller percentage of D_e values are at the maximum compared to Fig. 8. The LWP values (Fig. 11f) also show a greater range than seen in Fig. 9, with many values exceeding 50 gm^{-2}. These differences in the character of the results suggest that some input variables used in the NCOMP still need to be examined closely, especially the surface emissivities and radiative transfer calculations. Earlier version of NCOMP were also hampered by using the nominal SEVIRI 3.9-µm channel calibration. The impact of this assumption is discussed in 4.2.1.3.

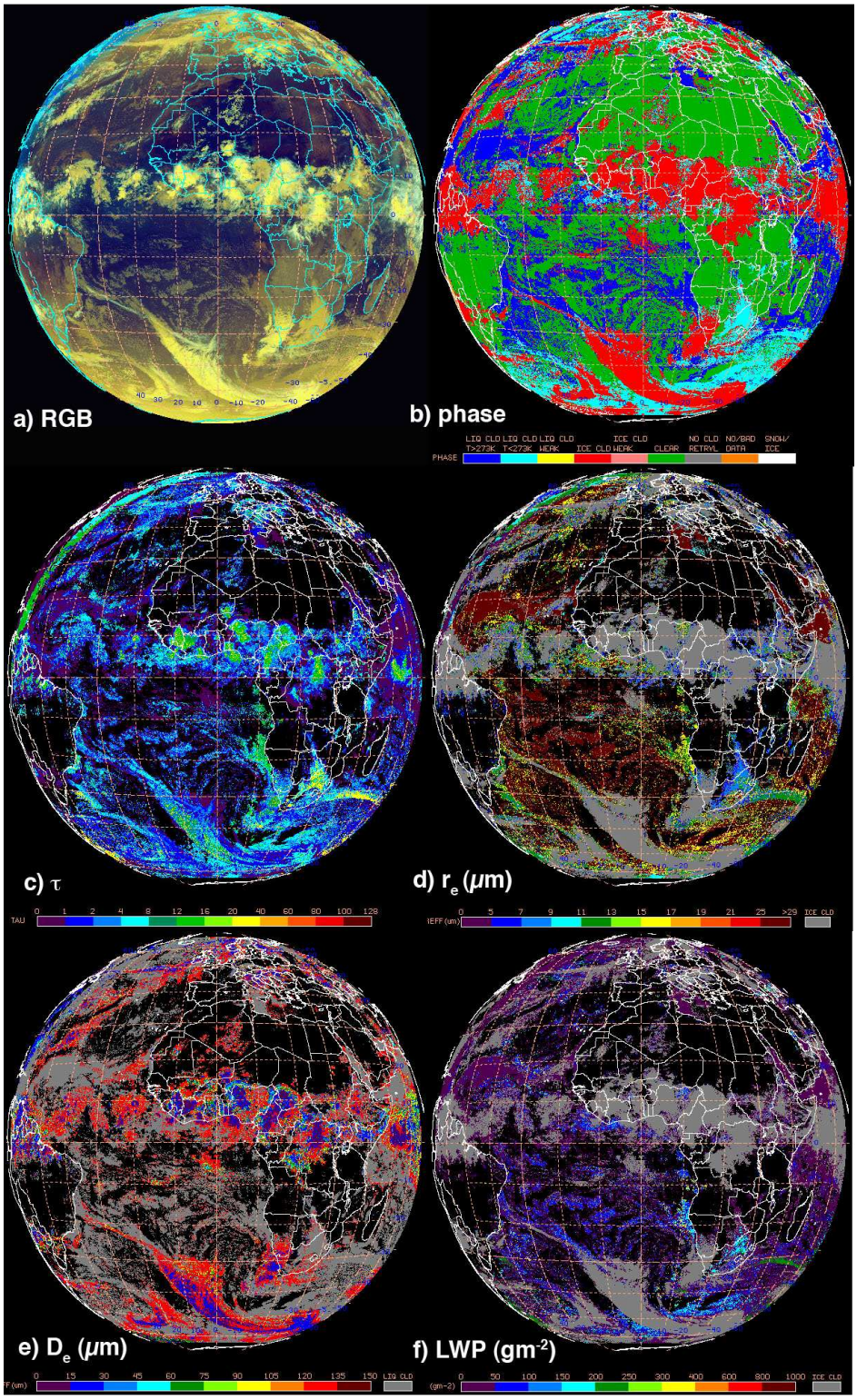

Figure 11. Cloud properties retrieved from Meteosat-9 SEVIRI using the SIST, 2215 UTC, 17 June 2008.

4.2.1 Precisions and Accuracy Estimates

The precision and accuracy of the results of the NCOMP can be determined both theoretically through sensitivity studies and via comparison with independent, presumably, more accurate measurements.

A set of sensitivity studies was conducted to fully define the accuracy and precision of each retrieved parameter. The results indicate that both accuracy and precision specifications are being met. These analyses explored the sensitivities of the retrievals to errors in surface emissivity and temperature and T_{cld}, and the cloud-surface temperature contrast for a wide range of conditions and particle sizes. These sensitivity studies, discussed in 4.2.2, enabled the specification of more reliable limits for the algorithm.

Uncertainties in the NCOMP cloud optical depth, particle size, LWP and IWP can be also be estimated by quantitative comparisons with coincident data from several sources:

1. Surface-based remote retrievals
2. Aircraft-based in situ retrievals
3. Satellite-based remote retrievals

As with any property retrieved from satellite instruments, direct comparisons can be difficult due to time and space matching issues, differences in algorithm assumptions and spectral variations. Regardless, extensive validation of NASA Langley's SIST has been performed using the full SIST algorithm. Once any inconsistencies between SIST and NCOMP results from the offline framework have been identified and eliminated, it is anticipated that the NCOMP validation effort will yield similar results as the algorithms' underpinnings are the same.

4.2.1.1 Cloud Optical Depth

Cloud optical depth and r_e can be estimated directly by flying an aircraft through a target cloud a making complete vertical profiles of cloud particle sizes and number densities [e.g., Eq. (3)]. Historically, such profiles are few and far between during daytime. Even rarer is the nocturnal profile. Thus, for comparison to NCOMP retrievals, τ and r_e have to be determined indirectly from remote sensing instruments. A variety of techniques (e.g., Liu and Illingsworth, 2000; Dong and Mace, 2003; Mace et al., 2005) have been developed to use uplooking microwave radiometers, lidars, cloud radars, and infrared radiometers to retrieve LWP/IWP and r_e, and, hence, τ. Even multispectral infrared radiometers have been used alone to retrieve τ and r_e for semi-transparent clouds without the aid of other instruments (e.g., Turner and Holz, 2005). Such measurements have been

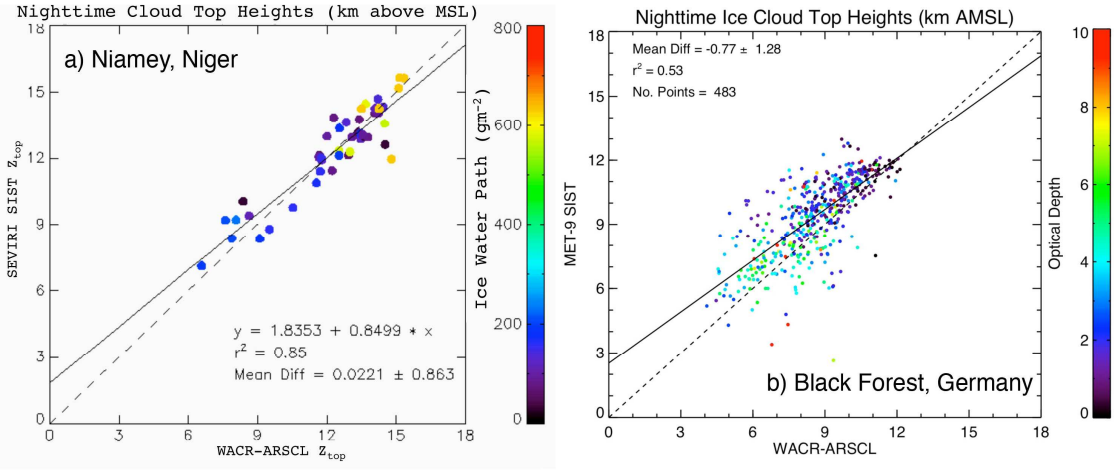

Figure 12. Comparison of SIST cloud top heights (km) from SEVIRI data and surface-measured cloud top heights from the AMF active sensors. (a) April – October 2006, SIST-derived IWP shown in color. (b) April – December 2007, SIST optical depth shown in color.

used extensively for daytime comparisons and should be applied more often to nocturnal retrievals. Lidars at the surface and on aircraft and satellites are all also used to retrieve thin cloud optical depths and particle sizes (e.g., Chiriaco et al., 2004, 2007). The infrared optical depths of optically thin clouds can be inferred from the heights of clouds. Thus, if the derived height is correct after correcting for semi-transparency, then τ must also be correct.

An example of that last approach is seen in Figure 12, which shows comparisons of ice cloud height obtained using SIST applied to SEVIRI imagery and from surface-based remote retrievals using combined radar, lidar and ceilometer products over the Atmospheric Radiation Measurement (ARM) Program Mobile Facility (AMF) when it was deployed at Niamey, Niger from April - October 2006 and over a site in the Black Forest in Germany from April - December 2007. The accuracy of the cloud heights for these ice clouds indicates that cloud optical depths are also quite accurate given that the cloud temperature is directly related to the cloud optical depth and emittance.

A similar comparison of cloud heights was performed over the ARM Southern Great Plains (SGP) by Smith et al. (2008) and showed very good agreement between the radar and SIST cloud top heights from GOES for optically thin clouds, indicating good agreement in cloud optical depth for the thin clouds.

The cloud optical depths can also be compared with MODIS-derived optical depths and particle sizes from the Cloud and Earth's Radiant Energy System (CERES) project, which are derived with SIST. This data set covers the entire globe for many years hence the full disk of SEVIRI results will be able to be compared with the MODIS optical depths. The comparison will provide a multitude of consistency checks as well as a validation of NCOMP's ability to produce similar results for multi-angle views of the same scene. Another consistency check is determine if the optical depths change

drastically between day and night in the absence of a pronounced, rapidly changing convective cycle. For example, Fig. 13 shows an example of the mean τ and r_e for liquid

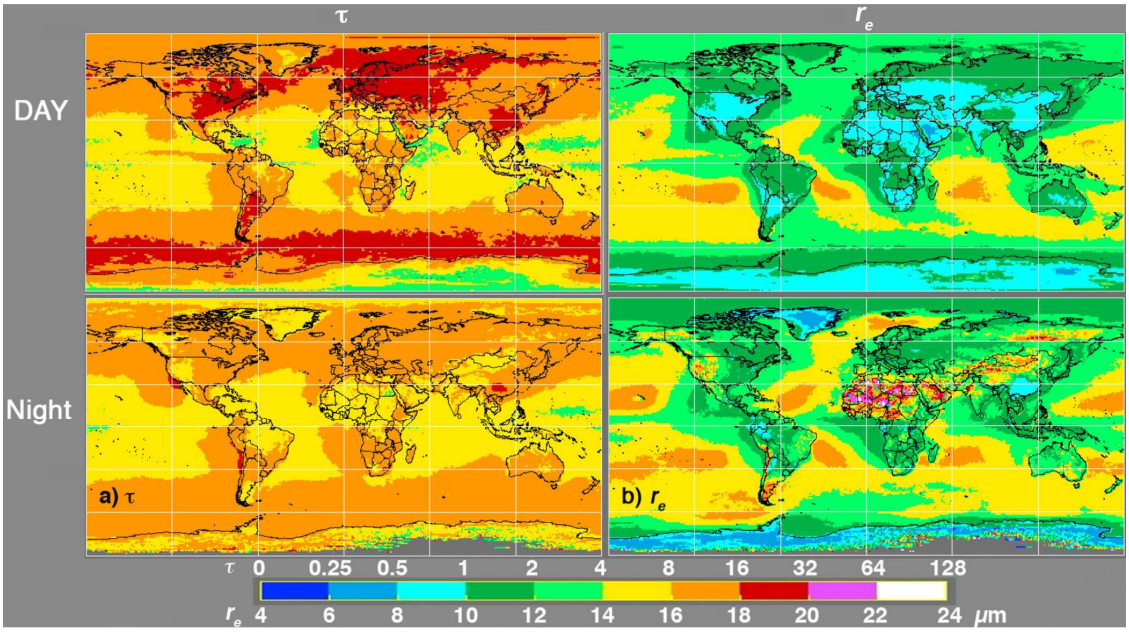

Figure 13. Mean liquid water optical depths and effective droplet radii derived from Terra MODIS data for CERES using the VISST (day) and SIST (night), 2001-2006.

water clouds derived from Terra MODIS data using the VISST during daytime (top row) and SIST at night (bottom row). Keeping the optical depth and particle size limitations of the SIST, the patterns in the mean values of both parameters are quite consistent over ocean. Over land areas, there is less consistency owing to the variability in ε_s and uncertainties in T_s, especially over deserts.

4.2.1.2 Cloud Particle Size

Figure 14 shows a case study comparison of ice cloud τ and r_e obtained using SIST applied to GOES imagery and analogous quantities derived from surface-based remote measurements using a surface-based interferometer (AERI) and Raman lidar (CARL) over the ARM Southern Great Plains (SGP) site for 2 nights, 8 November 2000 (Fig. 14a) and 29 November 2002 (Fig. 14b). The cloud boundaries from the lidar are also shown. The optical depths from satellite, indicated by the red diamonds, compare very well with the surface-based optical depths from AERI and CARL.

The AERI-derived particle sizes, while exhibiting a great deal of variation over this time scale, also compare fairly well with the SIST-derived r_e, although the absolute accuracy is difficult to assess given the high temporal resolution of the AERI and the low temporal resolution of GOES.

An example of comparisons with liquid water clouds is shown in Fig. 15 for data taken over the ARM SGP site for cases of overcast stratus clouds corresponding to Aqua MODIS overpasses. The SIST retrievals are shown as the solid symbols. The open symbols represent the retrievals from the surface using the method of Dong and Mace

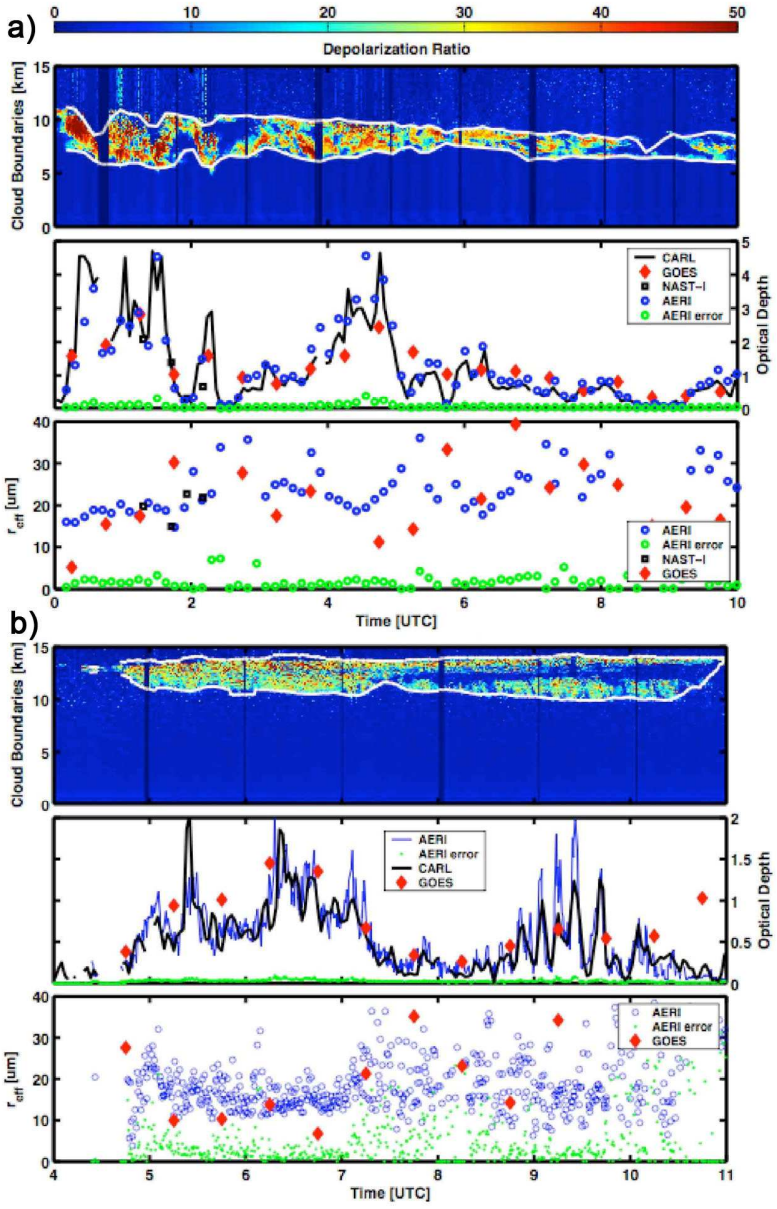

Figure 14. Comparison of SIST cloud optical depths and cloud particle sizes from GOES data and surface-measured quantities from surface interferometer (AERI) and Raman lidar (CARL) at the ARM SGP. (a) 8 November 2000. (b) 29 November 2002. CARL depolarization and cloud boundaries are shown in the top panels (personal communication, D. Deslover).

(2003) applied to the ARM radar and microwave radiometer data. On average, there is excellent agreement between results, but the correlation is relatively low. The highest squared correlation coefficient, found for τ, is 0.4. Greater correlation is found for all parameters, if only thinner clouds are compared. Similar datasets have been taken by the AMF over Germany and can be used in the same type of analysis to help validate the SEVIRI retrievals.

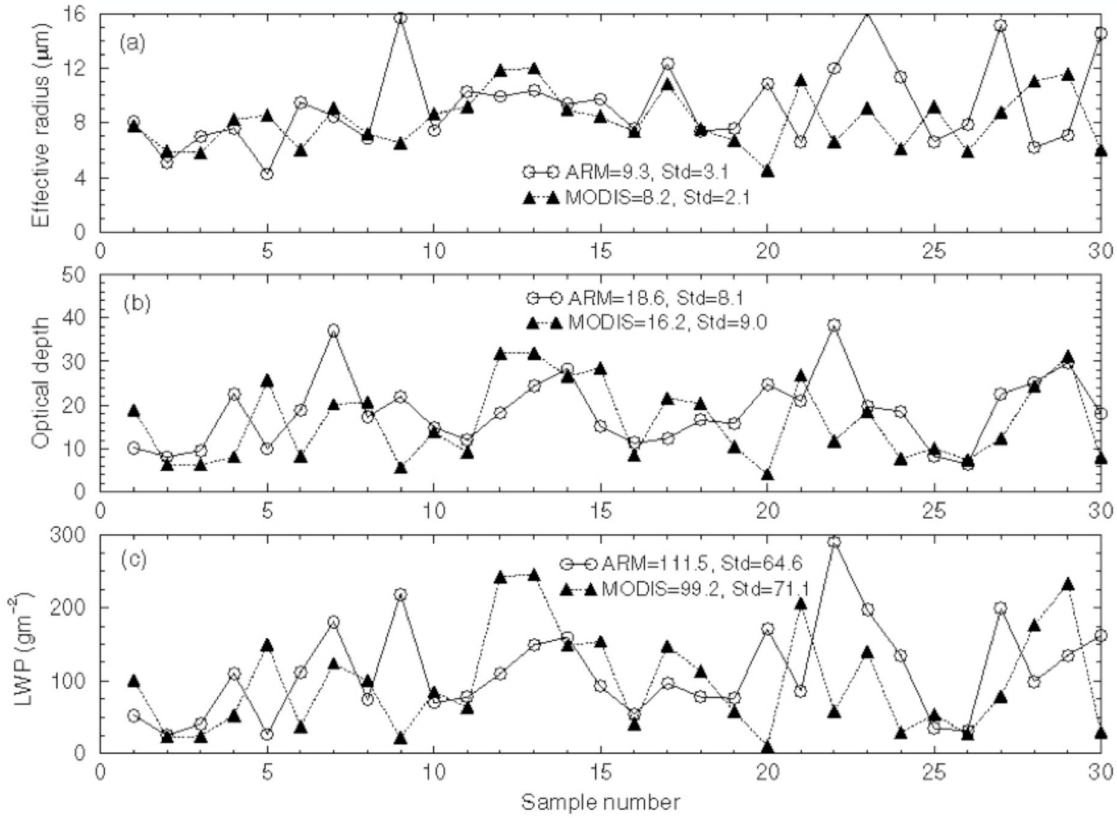

Figure 15. Comparison of mean cloud properties over the ARM SGP using surface-based measurements (ARM) and the SIST (MODIS) applied to nocturnal Aqua MODIS data, 2002-2005, for single-layer overcast stratus clouds. Each point represents a 15-min average from the surface data and a 30 km x 30 km average of satellite pixels. (personal communication, X. Dong).

4.2.1.3 LWP and IWP

The LWP and IWP retrieved from SIST have been compared with surface and airborne data as described above. As with the other NCOMP output, the liquid water path and ice water path can also be compared with MODIS-derived LWP and IWP from the CERES project, also derived with SIST or from SEVIRI using SIST. An added benefit of comparing NCOMP and SIST results to each other is that consistency checks can reveal any retrieval artifacts due to instrument calibration issues. A comparison of NCOMP and SIST IWP derived from the same SEVIRI images over Europe over 3-4 August 2006 is shown in Figure 16. An easily identifiable feature in comparing these results of IWP to

each other is an apparent bias, particularly at the higher values of IWP for thicker ABI Cloud Types of Ice and Overlap. As there is no spatial or temporal discontinuity to contend with, a fair conclusion might be that NCOMP has a high bias with respect to the better-validated SIST IWP retrievals.

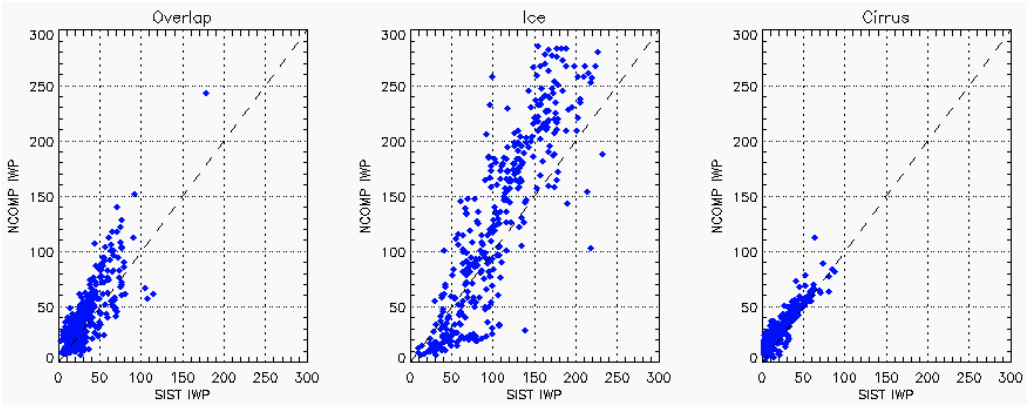

Figure 16. Comparison of NCOMP and SIST IWP for 3-4 August 2006 over Europe, separated by ABI Cloud-Type.

The bias, however, appears to be primarily the result of calibration differences. The SIST retrievals were performed in NASA Langley's framework utilizing recalibrated data while the NCOMP retrievals were conducted in the GOES-R developmental framework using the nominal SEVIRI calibrations for each channel. The NASA processing uses a robust calibration correction (Minnis et al., 2006) to the 3.9-μm channel that is based on comparisons between GOES-12 and SEVIRI with an example shown in Figure 17. The slope of the intercalibration appears to be almost identical to that of the IWP

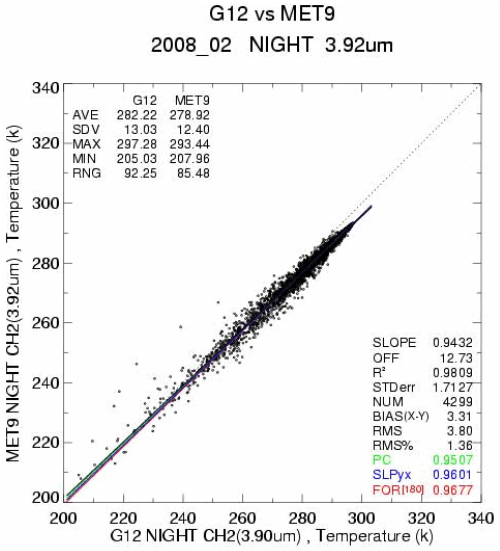

Figure 17. Calibration between spatially and temporally matched nighttime GOES-12 (G12) 3.9-µm temperatures and SEVIRI (MET9) 3.9-µm temperatures from NASA Langley.

comparison in Fig. 16, indicating that calibration discrepancies are contributing to an overestimation of NCOMP IWP. Given that 3.9-μm temperature differences as large as 4 K are expected, the bias in IWP has been reduced significantly by implementation in the GOES-R developmental framework for NCOMP (not shown). Due to the impact of calibration differences, the ability to modify radiances has been integrated into the NCOMP (see description of the Calibration Coefficients in 3.3.2).

Other efforts for validation of LWP and IWP are discussed in 5.5.3.

4.2.2 Error Budget

The error budget relies both on the retrieval validation and on the accuracies of several of the input parameters, as well as the parameterization uncertainties. The accuracy and precision estimates were developed based on detailed sensitivity studies and available empirical comparisons are analyzed in detail, but current results are presented in Table 6. The accuracies and precision estimates are extracted from the discussion of 5.5. While some of the requirements for which no direct comparison is indicated, we anticipate being able to complete them using limited case study-derived data because more thorough data sets are not available. The sensitivity analyses are presented below.

Table 6. Current NCOMP Accuracy and Precision Estimates Compared to F&PS Requirements. Red values indicate current NCOMP performance while * indicates a preliminary result that is further discussed in 5.5.

Product	*Measurement Range*	*Measurement Accuracy*	*Measurement Precision*
COD	1.0 – 5.0 1.0 – 5.0	30% 0.8%	max of 0.8 or 30% 0.46 or 29.7%
CPS	liquid: 2 < CPS < 32µm 2 < CPS < 32µm ice: 2 < CPS < 50µm 2 < CPS < 78µm	liquid: max of 4µm or 30% *no direct comparison ice: 10µm *10.2 µm	liquid: max of 4µm or 25% *no direct comparison ice: max of 10µm or 25% *43.9%
LWP	25 < LWP < 100 gm^{-2} 25 < LWP < 100 gm^{-2}	greater of 25 gm^{-2} or 15% 4.5 gm^{-2} or 4.1%	greater of 25 gm^{-2} or 40% 15.7 gm^{-2} or 30.4%
IWP	25 < IWP < 175 gm^{-2} 25 < IWP < 175 gm^{-2}	greater of 25 gm^{-2} or 30% *no direct comparison	greater of 25 gm^{-2} or 40% *no direct comparison

A detailed sensitivity analysis was performed for the NCOMP algorithm using the uncertainties expected in the input variables from upstream in the process. A Jacobian analysis was used wherein the brightness temperature for each channel was first calculated for the unperturbed case and then recalculated using the perturbation

corresponding to the input parameter uncertainties. In some cases a larger value was used and interpolation was employed to arrive at the true uncertainty value. Uncertainties in the surface emissivity (± 0.02), surface skin temperature (± 2.5 K), relative humidity (±15%), and T_{cld} (± 2 K for water, ± 3.5 K for ice) were considered. Calibration errors are considered small by comparison and were not evaluated. The calculations were performed using local zenith angles between 25 and 55° using standard atmospheric profiles and a range of COD and CPS for both ice and water clouds.

Each error was considered individually and in combination as random errors to obtain the RMS uncertainty resulting from errors in the input values. The sensitivity analysis is summarized in Fig. 18 for water and ice clouds separately. The COD errors vary between 22 and 28% for water clouds (Fig. 18a) and 15 and 32% for ice clouds (Fig. 18b). The

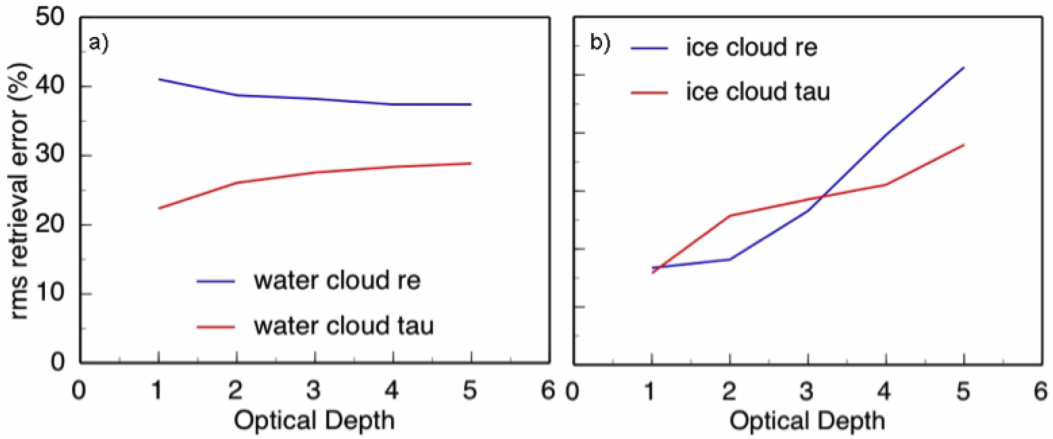

Figure 18. Summary of sensitivity errors of NCOMP COD and CPS (re), shown as RMS error of all input uncertainties combined. Larger errors were obtained for COD outside the range of 1 – 5.

errors increase rapidly for COD > 5 and COD < 1, particularly for ice clouds. The retrieved CPS errors are somewhat larger, around 40% for water and between 15 and 42% for ice CPS. The average ice cloud CPS RMS error is ~25%. These uncertainties meet both the current and pending F&PS requirements in most cases. The only exception is the water CPS.

5 PRACTICAL CONSIDERATIONS

5.1 Numerical Computation Considerations

The NCOMP is implemented sequentially. Because the algorithm relies on the values of the ancillary data, the radiative transfer model, NWP data set and the performance of the Cloud Height/Temperature and Cloud Phase/Type algorithms, these quantities need to be computed first.

5.2 Programming and Procedural Considerations

NCOMP is purely a pixel by pixel algorithm and requires no knowledge of the ABI radiances or cloud properties of the adjacent pixels. Results will not vary if larger or smaller amounts of imagery are processed. Several iterative steps are involved in NCOMP, but these are well tested in an operational setting. No forward calculations or look-up tables are required other than the calibration and emittance parameterization coefficients.

5.3 Quality Assessment and Diagnostics

The following quality assessment information in the form of the quality and processing flags of Table 7 and Table 8, respectively, are used to monitor the performance of the NCOMP. A Quality Flag of 0 indicates that the retrieval was performed successfully while a non-zero value indicates that a retrieval was not performed with the reason given by the values detailed in Table 7. The Processing flags are used for all pixels for which successful retrieval was performed. A non-zero Processing Flag bit reflects the path taken in the algorithm or what may be a physically important consideration, as in Table 8. Multiple Processing bits can be turned on because the algorithm paths are not independent.

In Table 7 the Quality Flag values are self-explanatory with the exception of the values of 6 or 7. These values are not likely to occur, but if there were to be a problem reading in the emittance parameterization coefficients described in 3.3.2 indicate that there is likely a problem either with the ingestion of the coefficients or with the coefficients themselves.

The Processing Flag values in Table 8 provide valuable validation information as well as tools for the user who may need to know how a particular solution was chosen. For example, if Processing Flag bit 1 is turn on, then the pixel is from twilight when NCOMP provides only qualitative results that are not expected to meet the F&PS requirements. In these situations the cloud properties are indeed present, but users will need to understand that they are potentially of a degraded quality. Other Processing Flag bits provide the potential for feedbacks between NCOMP's minimum error solution, described in 3.4.2.2, and the ABI Cloud Type. If the minimum error solution appears to be for a different

cloud type than indicated by the Cloud Type, then a bit is turned on. Similarly, if the potential for phase ambiguity is thought to be high, e.g., for overlap clouds, a Processing Flag bit will indicate this. Currently, this capability has no impact on the NCOMP cloud products other than the Processing Flag; it is simply an indicator that NCOMP is not yielding the best results for the situation described by the inputs or that the clouds are of a particular difficult variety.

Table 7. NCOMP Quality Flags.

Value	**Quality flag name**	**Cause & Effect**
Successful Retrieval Flag		
0	QC__GOOD	Successful retrieval
Angle Restriction Flags		
1	QC_CYCLE_VZA	Local Zenith Angle >= 72.0^{o}
2	QC_CYCLE_SZA	Solar Zenith Angle < 82.0^{o}
Ancillary Data Flags		
3	QC_CYCLE_NOCLOUD	Cloud Type indicates it is not a cloud
4	QC_CYCLE_CLOUDTYPE	Cloud Type has an unknown value
5	QC_CYCLE_TCLOUD	Cloud Temperature is < 0.0 (C)
No Retrieval Flags		
6	QC_MINERR_WATER_0	No retrieval: Minimum error model for water = 0
7	QC_MINERR_ICE_0	No retrieval: Minimum error model for ice = 0

Table 8. NCOMP Processing Flags.

Bit	**Processing flag name**	**Cause & Effect**
Valid Retrieval Flags		

1	QC_SZA_TWILIGHT_	82.0^o <= Solar Zenith Angle < 90.0^o
2	QC_CTWATER_NCOMPICE	Cloud Type = water, NCOMP preferred phase = ice
3	QC_CTICE_NCOMPWATER	Cloud Type = ice, NCOMP preferred phase = water
4	QC_CTMIX_NCOMPWATER	Cloud Type = mixed, NCOMP preferred phase = water
5	QC_CTMIX_NCOMPICE	Cloud Type = mixed, NCOMP preferred phase = ice
6	QC_CTSC_NCOMPWATER	Cloud Type = supercooled, NCOMP preferred phase = water
7	QC_CTSC_NCOMPICE	Cloud Type = supercooled, NCOMP preferred phase = ice
8	QC_CTOL_NCOMPWATER	Cloud Type = overlap, NCOMP preferred phase = water
9	QC_CTOL_NCOMPICE	Cloud Type = overlap, NCOMP preferred phase = ice
10	QC_MINERR_WATER_1	Minimum error model for water = 1
11	QC_MINERR_ICE_1	Minimum error model for ice = 1
12	QC_MINERR_WATER_LAST	Minimum error model or water = largest
13	QC_MINERR_ICE_LAST	Minimum error model for ice = largest
14	QC_TSURF_CHANGE	Temp_sfc from NWP used rather than from RTM

5.4 Exception Handling

The NCOMP includes checking the validity of the derived ABI inputs before applying the algorithm. The NCOMP expects the main processing system to flag any pixels with missing geo-location or solar and viewing geometry information.

The NCOMP does not check for conditions where the NCOMP cannot be performed or will return unreliable results, including saturated channels, missing RTM values or inconsistencies in the TRM data. In these cases, it is assumed that the framework will accomplish these tasks, particularly since NCOMP is late in the processing chain that many other algorithms will have already flagged such conditions, including those that provide derived ABI input to NCOMP. If explicit checking of every possible input is needed, this can easily be addressed.

The NCOMP returns no cloud properties if any of the required inputs, including channel data, are missing.

5.5 Algorithm Validation

In addition to the studies already mentioned, several additional comparisons have been performed to validate the results. Some comparisons use consistency, while others are direct quantitative comparisons. The types of comparisons reviewed in section 4.2.1 will continue to be repeated using offline framework-based NCOMP retrievals based on

SEVIRI data. After launch of GOES-R, surface sites in the Americas will be used for validations in addition to the use of other satellite data.

5.5.1 Cloud Optical Depth

Aligned with Aqua and CloudSat in the A-Train, the Cloud-Aerosol Lidar and Infrared Pathfinder Satellite Observation (CALIPSO) lidar is used to retrieve τ for clouds having $\tau < 3$. Comparisons with SEVIRI will be performed for every overpass for selected periods to assess the uncertainties in τ retrieved by the NCOMP. If CALIPSO or a similar instrument is in orbit after GOES-R is launched, its data will also be used to validate τ from the ABI. Additionally, it would be possible to simulate the ABI algorithm output by defining the cloud heights and temperatures using the CALIPSO and NWP temperature profiles and perform NCOMP on MODIS data matched to Aqua. The results could be compared to similar output from the method of Chiriaco et al. (2004) now being applied to CALIPSO lidar and infrared radiometer data.

A comparison of temporally and spatially matched NCOMP and CALIPSO optical depths from a subset of nighttime SEVIRI images taken the 10-week validation period is shown in Figure 18. The CALIPSO measurements are within ± 15 minutes of SEVIRI scan times and the SEVIRI pixel closest to each CALIPSO latitude and longitude, yet within 5 km, is chosen for the comparison. The range of τ plotted is limited to $1 \leq \tau \leq 5$ so that any statistics will be directly comparable to the F&PS requirements. While this τ limitation eliminates the majority of cloudy pixels from the comparisons, it is necessary due to the physical limitations of the current version of NCOMP which is reflected in the proposed requirements mentioned in 2.1.

The red points in Fig. 18 correspond to SEVIRI pixels with ABI Cloud Types of water, supercooled water, and cirrus, thought to be the most applicable to NCOMP's F&PS requirements, i.e., unambiguous phase, potentially optically thinner and apt to be single-layer. The black points are comprised of the remaining Cloud Types, hence are excluded from the statistical comparisons used to ascertain NCOMP's performance with respect to the requirements. The limited Cloud Type points in red have a bias (accuracy) of -0.451 while the black points have a bias of -0.662, corresponding to 35.2 and 50.6%, respectively, verifying that the subsetted Cloud Types show better agreement between NCOMP and CALIPSO although for both data sets NCOMP is generally higher. The limited value is still higher than the F&PS accuracy requirement of 30%, but further segmenting of the results is justified as explained below.

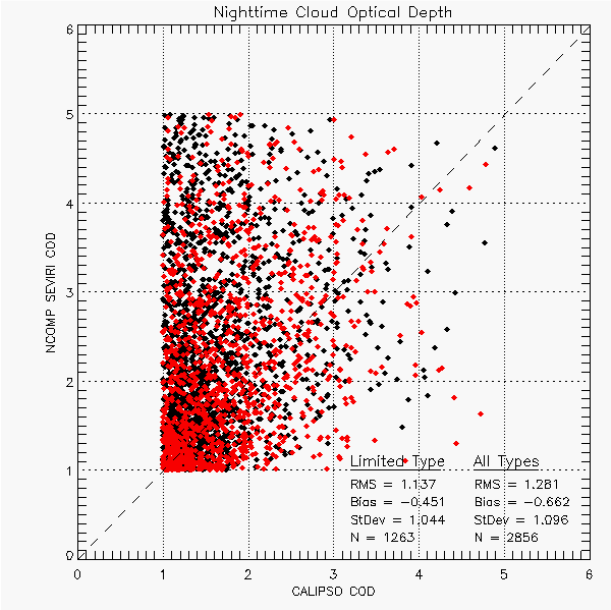

Figure 19. Comparison of matched NCOMP and CALIPSO COD from SEVIRI for a selection of images in the 10-week validation period.

The percentage difference of COD, CALIPSO – NCOMP, for each of the All Cloud Types points of Fig. 18 is shown in Fig. 19 as a function of CALIPSO COD. It is apparent that the cirrus points, despite generally having the lowest CODs, also have the best agreement with CALIPSO. The overlap clouds also have relatively low differences, despite the fact that the Cloud Type algorithm indicates that they are thin ice clouds over lower water clouds, a situation in which one might conclude that NCOMP would not perform well given its single-cloud layer assumption. The CALIPSO retrieval, however, generally does not include much of the impact of that lower layer as CALIPSO-derived water cloud information is not reliable, so in effect the overlapped pixels are somewhat similar to the cirrus points but with larger τ. Similarly, Cloud Types that are indicative of a water phase, fog, water, supercooled and mixed are also excluded from the eventual statistical comparisons. When Cloud Type = Ice in Fig. 19 the differences are also larger than for optically thin ice clouds (Cloud Type = Cirrus) because these pixels are assumed to be optically thick. While many of these points (dark blue) have CALIPSO COD well under 5, the reliability of those retrievals is questionable due to ongoing calibration and reprocessing issues associated with CALIPSO retrievals and algorithmic shortcomings, so these are also eliminated from that statistics. As indicated by one of the CALIPSO Program scientists, liquid water cloud optical depths are not reliable (C. Trepte, personal communication, 2009). Thus, the only statistics that have merit for this comparison are those for semitransparent ice clouds. Those statistics are reported in Table 6.

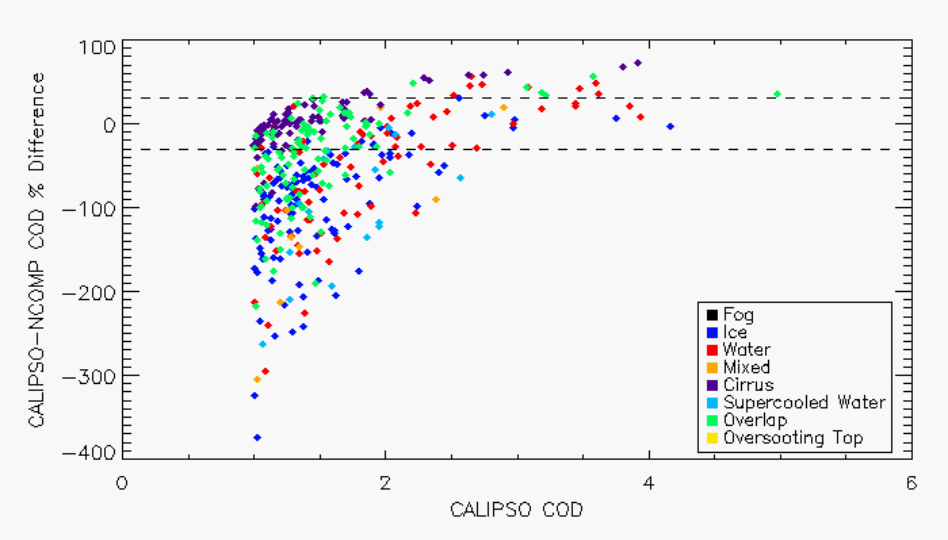

Figure 20. Percentage differences between NCOMP and CALIPSO COD for data in Fig. 18 with ABI Cloud Type indicated by color.

Using only the most reliable CALIPSO COD points in Fig. 19, those associated with ABI Cloud Type of Cirrus the bias has improved from -0.451 to +0.084 (or 1.32%), well under the required bias of 30%. For this same set of cirrus-only points, the accuracy is 0.49 or 30.0%, also within the required accuracy, the maximum of 0.8 or 30%.

For single-layer water clouds with $1 \leq \text{COD} \leq 5$, ongoing comparisons with CloudSat-derived COD continue be an option for validation, but first comparisons have not yielded sufficient results. This is expected for several reasons, but the largest hindrance is CloudSat's usage of Radar-Only (RO) retrieval techniques at night. During daylight hours when MODIS algorithms do retrieve COD, CloudSat uses MODIS COD to constrain and bolster the RO retrieval, providing superior results, but at night there are no MODIS retrievals of COD, so CloudSat products are still considered experimental and evolving due to the limitations of the RO technique. Additional source of error are CloudSat's inability to detect some optically thin clouds and water clouds with bases below 1 km, as all as NCOMP's relatively small range of retrievable CODs.

Data from well-equipped surface observatories in Europe (Illingworth et al., 2007) as well as the AMF campaign datasets (e.g., Niamey and Black Forest) discussed earlier will continue to be used to validate SEVIRI NCOMP optical depth retrievals using the various methods mentioned in section 4.2.1. Unfortunately, the existing amount of surface data available in the SEVIRI field of view is very limited, particularly when choosing from the 10-week SEVIRI validation period. Validation using surface data will be extended to other time periods to take advantage of these sparse, but relatively well-tested validation sources for COD, as well as LWP, and potentially CPS and IWP. Post-launch data from the ARM sites could also be used for comparison with the ABI retrievals.

A less quantitative, yet useful method for validating the results is by comparing the nighttime retrievals to the nearest daytime retrievals over the same area. Figure 20 shows an example of the daytime VISST and nighttime SIST applied to SEVIRI data at 1500 and 1800 UTC, 6 August 2009. SIST results were used rather than NCOMP because the NCOMP twilight retrievals are required only to be qualitative, hence not as robust as the more reliable twilight SIST retrievals, and because direct comparison was easier due to VISST being run only in a NASA Langley framework. The RGB images (Figs. 20a and b) show the terminator and the cloud structure quite distinctly. Off the east coast of southern Africa, the structure of the low-cloud optical depths is maintained relatively intact although τ has decreased overall. The high clouds to the south, which had relatively large values of τ at 15 UTC, have maximum values of only $\tau = 4$ at 18 UTC. This drop in the high cloud optical depths is likely due to much of the high cloud cover being relatively thin and over optically thick low clouds. Thus, during the daytime, the total optical depth is retrieved, while, at night, only the high cloud optical depth is retrieved because the value of T_{cld} from using the 13.3-µm channel (similar to the ABI algorithm) was used in these SIST retrievals. The identification of most of these clouds as multi-layered (Fig. 21) using the algorithm of Chang et al. (2009) confirms the result. In other areas (e.g. central Africa) where high clouds were optically thick from deep convective activity, the patterns in τ follow the thick clouds seen in the RGB image (Fig. 20b) and in the 15-UTC τ image (Fig. 20c).

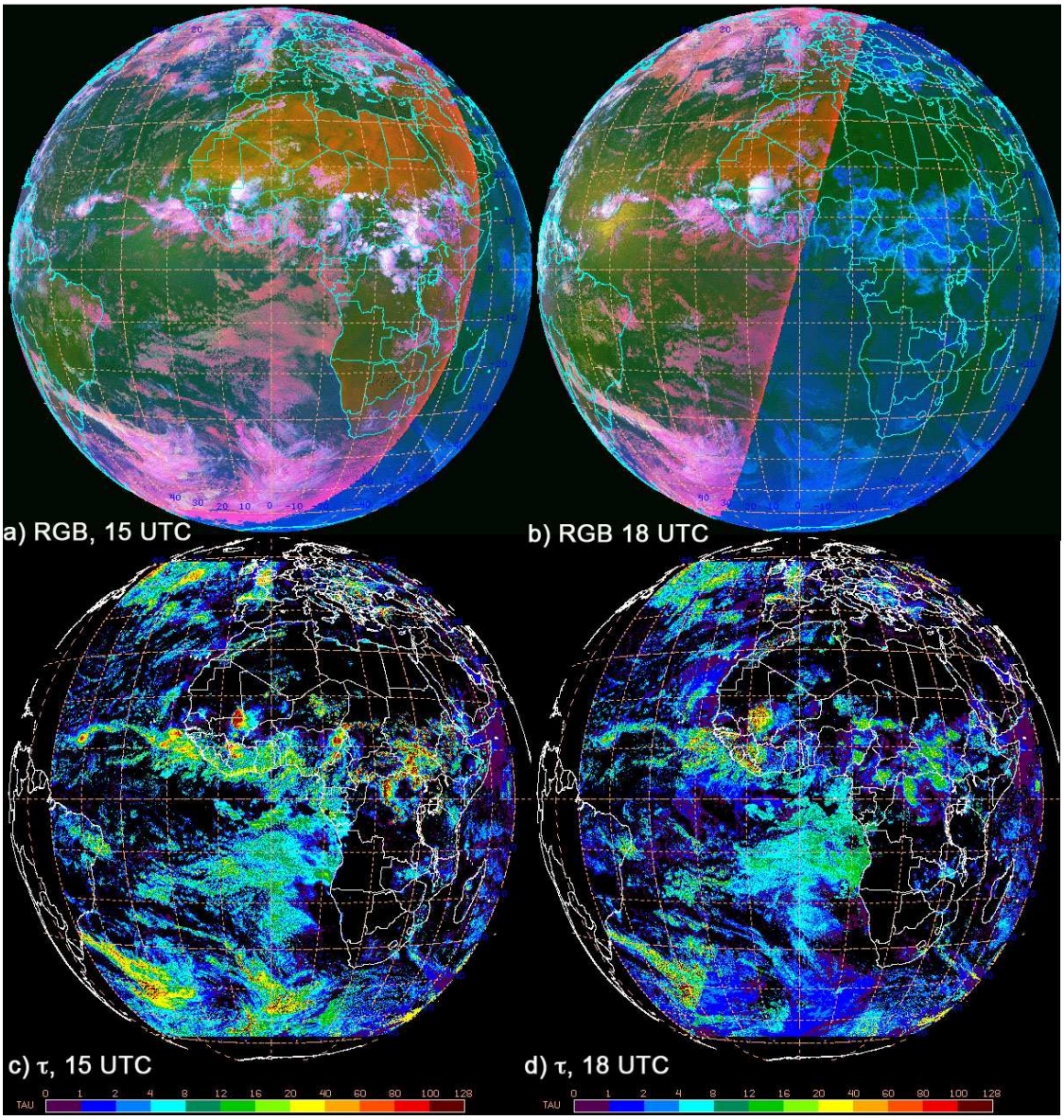

Figure 21. Meteosat-9 SEVIRI imagery (RGB) and retrieved cloud optical depths (τ), 6 August 2009.

The examples in Figs. 20 and 21 show how sequences of data can be used to quickly evaluate the results to determine where and in what conditions the algorithm fails or gives unexpected results. Use of hourly or more frequent sequential images and output parameters will be valuable for rapid visual assessment of the NCOMP output so that potential problem areas can be identified and selected for further study.

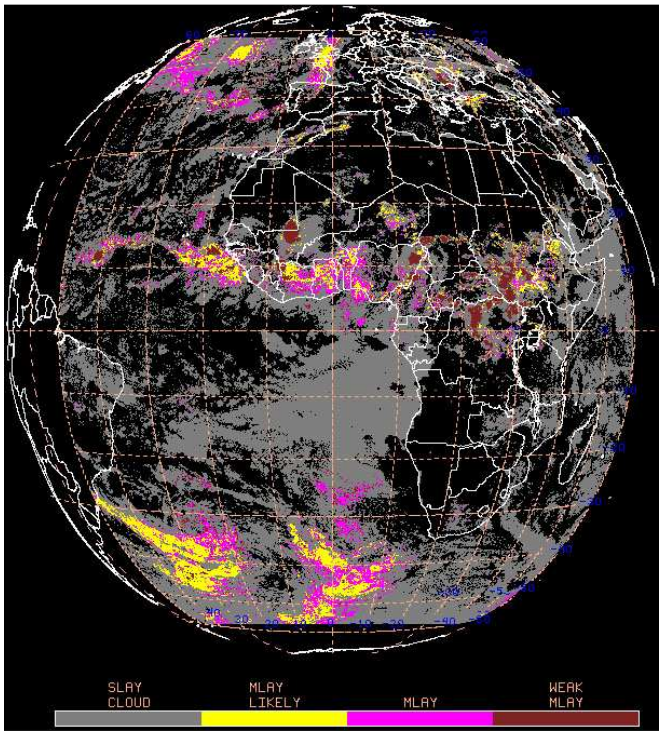

Figure 22. Multi-layered cloud probability, SEVIRI, 15 UTC, 6 August 2009. Gray denotes single-layered clouds, yellow: likely multi-layered clouds, magenta: definite multilayered clouds, brown: possible multilayered clouds, but more likely, a very thick contiguous water-ice cloud system.

5.5.2 Cloud Particle Size

The validation of cloud particle size will follow the same path used to evaluate the optical depth. In most cases, the assessments will be performed on both parameters using the same datasets. Figure 22 shows the retrievals of ice (IWC) and liquid water content (LWC) and r_e profiles from radar and microwave radiometer retrievals over two

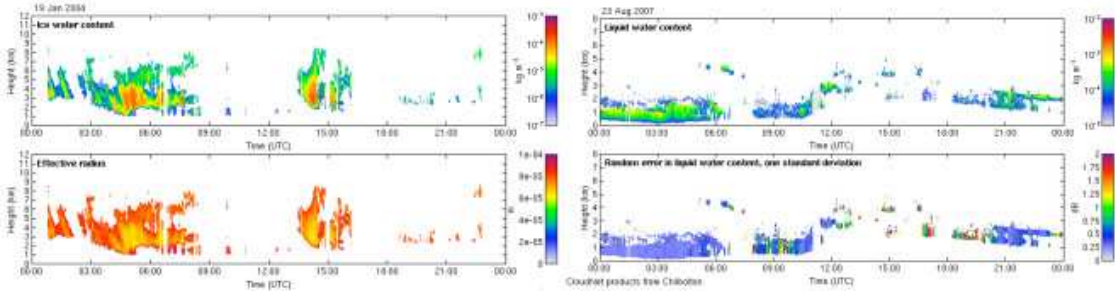

Figure 23. Retrievals of ice water content (top left) and r_e (bottom left) at Palaiseau, France, 19 Jan. 2004 and liquid water content (top right) and error (bottom right) at Chilbolton, UK, 23 Aug 2007.

CLOUDNET sites, SIRTA in Palaiseau, France (left panels) and Chilbolton, UK (right panels). The LWC and IWC profiles can be integrated over the cloud thickness to obtain LWP and IWP, respectively. In like manner, the column integrated r_e can be computed for comparison with the SEVIRI retrievals. This same approach can be used with ARM site data and the CloudSat GEOPROF products to provide more spatial sampling. Consistency checks will also be performed as discussed in the previous section.

Due to the surface sites containing only a single SEVIRI pixel, SEVIRI imagery from a large number of months and likely a large number of years will need to be processed with GOES-R cloud algorithms to provide statistically significant amounts of comparisons. Additionally, NCOMP's need to limit comparisons to only single-layer optically thin cases for either water are ice further reduces surface-based validation opportunities.

CloudSat CPS for GOES-R Cloud Types cirrus and water have been compared to CloudSat data during the 10-week validation period, using a method similar to the COD comparisons of 5.5.1. As with COD, the RO CloudSat technique and the still evolving CloudSat algorithms were expected to negatively influence the comparisons. For cirrus clouds with COD between 1 and 5, accuracy specifications were met (-0.2 µm) with the F&PS accuracy being 10 µm, but precision was only 43.9% with a requirement of 25%. Zhang and Mace (2006) found that RO retrievals of CPS have theoretical uncertainty ranging from 50 to 90%, so even this modest agreement is surprising. Generally though, this result indicates that nighttime CloudSat results are not likely to be a robust validation source.

5.5.3 LWP and IWP

Validation of IWP and LWP will also follow the same approaches used for r_e and τ since the parameters are all linked together. Thus, surface site and CloudSat profiles will be used for validating both IWP and LWP, while the CALIPSO IWC profiles for thin cirrus clouds can also be used for IWP evaluations. One additional dataset will be used to further validate the LWP over ocean, the LWP values retrieved from satellite-borne microwave radiometers. LWP is standard product from the AMSR-E on Aqua, TMI on TRMM, and SSM/I on the DMSP series of satellites. Those products can be easily matched with the results from the offline framework and compared with either SEVIRI or future ABI LWP retrievals.

A comparison of NCOMP LWP and AMSR-E LWP has been done for another subset of the 10-week validation period and is shown in Figure 23. Similar to the data shown in Figs. 18 and 19, this comparison was limited to those nighttime points with $1 \leq \tau \leq 5$. Additionally, given that many SEVIRI pixels were averaged together to mimic the AMSR-E footprint size, only those aggregate NCOMP points that contained at least 75% water clouds, based on the ABI Cloud Type, were included. While this limited the number of points, it did provide good comparison opportunities as the accuracy of these matches is 4.5 gm^{-2} and the precision is 15.7 gm^{-2}, both meeting the F&PS requirements of 25 gm^{-2} and 25 gm^{-2}, respectively. Greenwald et al. (2007) explore the uncertainties in the AMSR-E LWP retrievals, which are fairly large, so this result is encouraging.

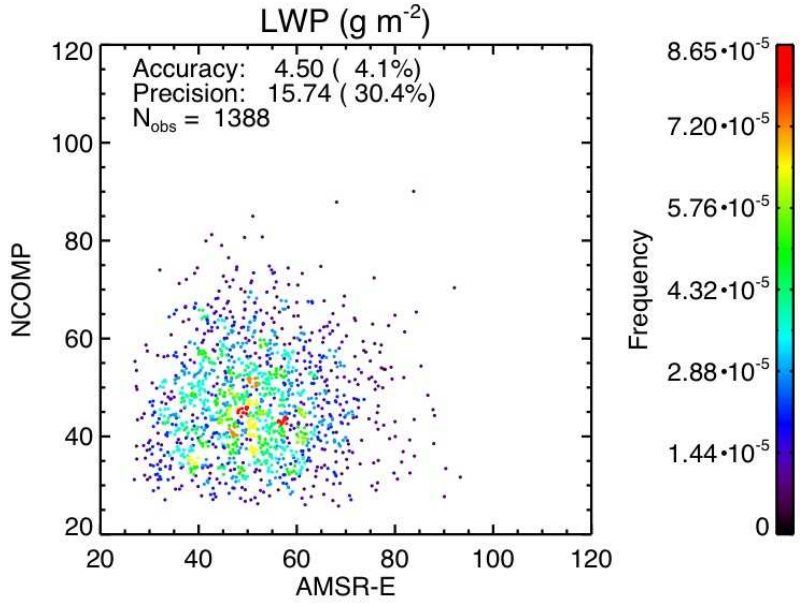

Figure 24. Retrievals of liquid water path (gm^{-2}) from matched AMSR-E and NCOMP from a subset of SEVIRI imagery during the 10-week validation period.

LWP and IWP from CloudSat was also compared to NCOMP during the same period. As with CloudSat CPS and COD, the RO limitations of CloudSat, as well as NCOMP's own uncertainty of 40%, are expected to limit the potential for these comparisons, yet LWP for GOES-R Cloud Type water yielded a bias of 14.0 g/m2 or 18.2% with accuracy of 24.9 g/m2 or 37.7%. While these LWP results are within the F&PS criteria, the number of samples was only 116 and perhaps fortuitous, so the AMSR-E comparisons from Fig. 23 are used in assessing NCOMP's LWP performance. As expected and as noted by Zhang and Mace (2006) who found theoretical RO IWP uncertainties of 40 to 50% , IWP comparisons with CloudSat yielded less impressive results.

The aforementioned linkage of LWP, CPS and COD indicates that those quantities proving difficult to validate, namely CPS and IWP, are expected to meet GOES-R specifications. Given that LWP is meeting F&PS criteria, despite thin water clouds often proving difficult for remote sensing techniques to quantify, we anticipate that if a sufficient source of surface data is identified, water cloud CPS and COD will compare well. Similarly, the ice cloud COD comparisons with Calipso, the gold standard sensor for thin ice clouds, are meeting specifications, so we anticipate that ice cloud CPS, hence IWP will also meet specifications.

Bolstering our validation is also possible by running the GOES-R algorithms on MODIS or GOES data, thereby greatly increasing the availability of surface sites that have MWR and MWR-radar combinations from which COD, CPS, LWP and IWP can be derived. Once those capabilities are available, these additional validations will be conducted.

6 ASSUMPTIONS AND LIMITATIONS

The following sections describe the current limitations and assumptions in the current version of the NCOMP.

6.1 Performance

The following assumptions have been made in developing and estimating the performance of the NCOMP. The following list contains the current assumptions and proposed mitigation strategies.

1. NWP data of comparable or superior quality to the current 6 hourly GFS forecasts are available. (Use longer range GFS forecasts or switch to another NWP source – ECMWF).

2. RTM calculations are available for each pixel. (Use reduced vertical or spatial resolution in driving the RTM).

3. All of the ancillary data is available at the pixel level. (Use larger scale ancillary date sets).

4. All required ABI channels are available.

6.2 Assumed Sensor Performance

We assume the sensor will meet its current specifications. However, the NCOMP will be dependent on the following instrumental characteristics.

1. Unknown spectral shifts in some channels will cause biases in the clear-sky RTM calculations and in the accuracy of the emittance parameterizations, which may impact the performance of the NCOMP.

2. Errors in navigation from image to image will affect the accuracy of clear sky temperatures that are used in the retrieval scheme.

As discussed earlier, calibration differences will be closely monitored.

6.3 Pre-Planned Product Improvements

The NCOMP development is tied to the development of other ABI algorithms. At this point, it is therefore difficult to predict what the future modifications will be. However, the following list contains our current best guess of the future NCOMP modifications.

6.3.1 Addition of Other Wavelengths

It is surmised that use of the SEVIRI 8.5- and 13.3-µm channels can provide additional information that can be exploited to improve the NCOMP retrievals (e.g., Takano et al., 1992; Strabala et al., 1994). Currently at NASA Langley, modifications to the SIST using the 8.5- and 13.3-µm channels are being studied, although usage of other channels cannot be ruled out. Results of those analyses using SEVIRI and MODIS data will determine whether or not the NCOMP will be modified. Use of additional wavelengths may allow NCOMP to determine optical depths for optically thicker clouds and may reduce inaccuracies in optical depth and particle size, hence LWP and IWP.

6.3.2 Multi-layer Clouds

The NCOMPS performance in situations with multi-layer clouds will be explored. If it is possible to include recent innovations in detecting multiple cloud layers (Chang et al., 2009) and the properties of the respective layers, then those techniques will be streamlined and adapted for NCOMP usage.

6.3.3 Parameterization Updates

The emittance parameterizations will be updated using the SEVIRI filter functions rather than GOES filter functions. Additionally, the usage of new ice crystal models that include rough crystals will be explored. Both of these should result in improved cloud optical depths and particle sizes. To maintain consistency with the daytime retrievals, a completely new set of models will also be developed that uses the official Cloud AWG ice crystal model set for ABI retrievals. They will be thoroughly tested and validated as well as produced in-house by NASA Langley.

7 REFERENCES

Baum, B.A., P. F. Soulen, K. I. Strabala, M. D. King, S. A. Ackerman, and W. P. Menzel, Remote sensing of cloud properties using MODIS Airborne Simulator imagery during SUCCESS, 2000. II. Cloud thermodynamic phase. *J. Geophys.Res.*, **105**, 11,781-11,792.

Chang, F.-L., P. Minnis, B. Lin, M. Khaiyer, R. Palikonda, and D. Spangenberg, 2009: A modified method for inferring cloud top height using GOES-12 imager 10.7- and 13.3-µm data. Submitted to *J. Geophys. Res.*

Chiriaco, M., H. Chepfer, P. Minnis, M. Haeffelin, S. Platnick, D. Baumgardner, P. Dubuisson, M. McGill, V. Noel, J. Pelon, D. Spangenberg, S. Sun-Mack, and G. Wind, 2007: Comparison of CALIPSO-like, LaRC, and MODIS retrievals of ice cloud properties over SIRTA in France and Florida during CRYSTAL-FACE. *J. Appl. Meteorol. Climatol*., **46**, 242-272.

Chiriaco, M., H. Chepfer, V. Noel, A. Delaval, M. Haeffelin, P. Dubuisson, and P. Yang. 2004. Coupling infrared radiometer and lidar observations for retrieving semi-transparent cirrus cloud particle size. *Mon. Wea. Rev.*, **132**, 1684-1700.

Dong, X., and G. G. Mace, 2003: Profiles of low-level stratus cloud microphysics deduced from ground-based measurements. *J. Atmos. Oceanic Tech.*, **20**, 42-53.

Downing, H. D. and D. Williams, 1975: Optical constants of water in the infrared. *J. Geophys. Res*., **80**, 1656-1661.

Greenwald, T. J., T. S. L'Ecuyer, and S. A. Christopher, 2007: Evaluating specific error characteristics of microwave-derived liquid water cloud products. *Geophys. Res. Lett.*, 34, L22807, doi:10.1029/2007GL031180.

Hansen, M., R. DeFries, J.R.G. Townshend, and R. Sohlberg, 1998: UMD Global Land Cover Classification, 1 Kilometer, 1.0, Department of Geography, University of Maryland, College Park, Maryland, 1981-1994.

Illingworth, A. J., and Co-authors, 2007: CLOUDNET, continuous evaluation of cloud profiles in seven operational models using ground-based observations. *Bull. Amer. Meteorol. Soc.*, **88**, 883-898.

Katagiri, S. and T. Nakajima, 2004: Characteristics of cirrus clouds as retrieved from AVHRR. *J. Meteorol. Soc. Japan*, **82**, 81-89.

Lin, X., and J. A. Coakley, 1993: Retrieval of properties for semitransparent clouds from multispectral infrared imagery data. *J. Geophys. Res*., **98**, 18,501-18,514.

Liu, C.-L., and A. J. Illingworth, 2000: Toward more accurate retrievals of ice water content from radar measurements of clouds. *J. Appl. Meteorol*., **39**, 1130-1146.

Mace, G. G., Y. Zhang, S. Platnick, M. D. King, P. Minnis, and P. Yang, 2005: Evaluation of cirrus cloud properties from MODIS radiances using cloud properties derived from ground-based data collected at the ARM SGP site. *J. Appl. Meteorol.,* **44**, 221-240.

Minnis, P., L. Nguyen, W. L. Smith, Jr., R. Palikonda, D. R. Doelling, J. K. Ayers, Q. Z. Trepte, and F.-L., Chang, 2006: MSG SEVIRI applications for weather and climate: Cloud properties and calibrations. *Proc. 3rd MSG RAO Workshop,* (ES SP-619) Helsinki, Finland, June 15, 25-30.

Minnis, P., D. P. Garber, D. F. Young, R. F. Arduini, and Y. Takano, 1998: Parameterization of reflectance and effective emittance for satellite remote sensing of cloud properties. *J. Atmos. Sci.*, **55**, 3313-3339.

Minnis, P., D. P. Kratz, J. A., Jr. Coakley, M. D. King, D. Garber, P. Heck, S. Mayor, D. F. Young, and R. Arduini: Cloud Optical Property Retrieval (Subsystem 4.3). "Clouds and the Earth's Radiant Energy System (CERES) Algorithm Theoretical Basis Document, Volume III: Cloud Analyses and Radiance Inversions (Subsystem 4)", NASA RP 1376 Vol. 3, edited by CERES Science Team, December, 1995, pp. 135-176.

Minnis, P., K. N. Liou, and Y. Takano, 1993: Inference of cirrus cloud properties using satellite-observed visible and infrared radiances. Part I: Parameterization of radiance fields. *J. Atmos. Sci.*, **50**, 1279-1304.

Minnis, P., and Co-authors, 2009: Cloud property retrievals for CERES using TRMM VIRS and Terra and Aqua MODIS data. *IEEE Trans. Geosci. Remote Sens.*, submitted.

Seemann, S.W., E. E. Borbas, R. O. Knuteson, G. R. Stephenson, and H.-L. Huang, 2007: Development of a global infrared land surface emissivity database for application to clear sky sounding retrievals from multi-spectral satellite radiance measurements. *J. Appl. Meteorol. Climatol.*, **47**, 108–123

Smith, W. L., P. Minnis, H. Finney, R. Palikonda, and M. M. Khaiyer, 2008: An evaluation of operational GOES-derived single-layer cloud top heights with ARSCL over the ARM Southern Great Plains site. *Geophys. Res. Lett.*, **35**, L13820, doi:10.1029/2008GL034275.

Strabala, K. I., S. A. Ackerman, and W. P. Menzel, 1994: Cloud properties inferred from 8–12-µm data. *J. Appl. Meteor.*, **33,** 212–229.

Takano, Y., Liou, K. N. and P. Minnis, 1992: The effects of small ice crystals on cirrus infrared properties. *J. Atmos. Sci.*, **49**, 1487-1493.

Takano, Y. and K. N. Liou, 1989: Radiative transfer in cirrus clouds I. Single scattering and optical properties of oriented hexagonal ice crystals. *J. Atmos. Sci.*, **46**, 3-20.

Turner, D. D. and R. E. Holz, 2005: Retrieving cloud fraction in the field-of-view of a high-spectral-resolution infrared radiometer. *Geosci. Remote Sens. Lett.*, **3**, 287-291.

Warren, S. G., 1984: Optical constants of ice from the ultraviolet to the microwave. *Appl. Opt*., **23**, 1206-1224.

Zhang, Y. and G. Mace, 2006: Retrieval of cirrus microphysical properties with a suite of algorithms for airborne and spaceborne lidar, radar, and radiometer data. *J. Appl. Meteor. Clim.*, **45**, 1665-1689.

Appendix 1: Common Ancillary Data Sets

1. LAND_MASK_NASA_1KM

a. Data description

Description: Global 1km land/water used for MODIS collection 5
Filename: lw_geo_2001001_v03m.nc
Origin: Created by SSEC/CIMSS based on NASA MODIS collection 5
Size: 890 MB.
Static/Dynamic: Static

b. Interpolation description

The closest point is used for each satellite pixel:

1) Given ancillary grid of large size than satellite grid
2) In Latitude / Longitude space, use the ancillary data closest to the satellite pixel.

2. NWP_GFS

a. *Data description*

Description: NCEP GFS model data in grib format – 1 x 1 degree (360x181), 26 levels
Filename: gfs.tHHz.pgrbfhh
Where,
HH – Forecast time in hour: 00, 06, 12, 18
hh – Previous hours used to make forecast: 00, 03, 06, 09
Origin: NCEP
Size: 26MB
Static/Dynamic: Dynamic

b. Interpolation description

There are three interpolations are installed:

NWP forecast interpolation from different forecast time:

Load two NWP grib files which are for two different forecast time and interpolate to the satellite time using linear interpolation with time difference.

Suppose:

T1, T2 are NWP forecast time, T is satellite observation time, and T1 < T < T2. Y is any NWP field. Then field Y at satellite observation time T is:

$$Y(T) = Y(T1) * W(T1) + Y(T2) * W(T2)$$

Where W is weight and

$$W(T1) = 1 – (T-T1) / (T2-T1)$$
$$W(T2) = (T-T1) / (T2-T1)$$

NWP forecast spatial interpolation from NWP forecast grid points. This interpolation generates the NWP forecast for the satellite pixel from the NWP forecast grid dataset.

The closest point is used for each satellite pixel:

1) Given NWP forecast grid of large size than satellite grid
2) In Latitude / Longitude space, use the ancillary data closest to the satellite pixel.

NWP forecast profile vertical interpolation

Interpolate NWP GFS profile from 26 pressure levels to 101 pressure levels

For vertical profile interpolation, linear interpolation with Log pressure is used:

Suppose:

y is temperature or water vapor at 26 levels, and y101 is temperature or water vapor at 101 levels. p is any pressure level between p(i) and p(i-1), with p(i-1) < p <p(i). y(i) and y(i-1) are y at pressure level p(i) and p(i-1). Then y101 at pressure p level is:

$$y101(p) = y(i-1) + \log(p[i] / p[i-1]) * (y[i] – y[i-1]) / \log (p[i] / p[i-1])$$

3. SFC_TYPE_AVHRR_1KM

a. *Data description*

Description: Surface type mask based on AVHRR at 1km resolution
Filename: gl-latlong-1km-landcover.nc
Origin: University of Maryland
Size: 890 MB
Static/Dynamic: Static

b. *Interpolation description*

The closest point is used for each satellite pixel:

1) Given ancillary grid of large size than satellite grid
1) In Latitude / Longitude space, use the ancillary data closest to the satellite pixel.

4. SFC_EMISS_SEEBOR

a. *Data description*

Description: Surface emissivity at 5km resolution
Filename: global_emiss_intABI_YYYYDDD.nc
Where, YYYYDDD = year plus Julian day
Origin: UW Baseline Fit, Seeman and Borbas (2006).
Size: 693 MB x 12
Static/Dynamic: Dynamic

b. *Interpolation description*

The closest point is used for each satellite pixel:

1) Given ancillary grid of large size than satellite grid
2) In Latitude / Longitude space, use the ancillary data closest to the satellite pixel.

5. CRTM

a. Data *description*

Description: Community radiative transfer model
Filename: N/A
Origin: NOAA / NESDIS
Size: N/A
Static/Dynamic: N/A

b. Interpolation *description*

A double linear interpolation is applied in the interpolation of the transmissitance and radiance profile, as well as in the surface emissivity, from four nearest neighbor NWP grid points to the satellite observation point. There is no curvature effect. The weights of the four points are defined by the Latitude / Longitude difference between neighbor NWP grid points and the satellite observation point. The weight is defined with subroutine ValueToGrid_Coord:

NWP forecast data is in a regular grid.

Suppose:
Latitude and Longitude of the four points are:
(Lat1, Lon1), (Lat1, Lon2), (Lat2, Lon1), (Lat2, Lon2)
Satellite observation point is:
(Lat, Lon)

Define
aLat = (Lat – Lat1) / (Lat2 – Lat1)
alon = (Lon – Lon1) / (Lon2 – Lon1)

Then the weights at four points are:
w11 = aLat * aLon
w12 = aLat * (1 – aLon)
w21 = (1 – aLat) * aLon
w22 = (1-aLat) * (1 – aLon)

Also define variable at the four points are:
a11, a12, a21, a22

Then the corresponding interpolated result at satellite observation point (Lat, Lon) should be:

a(Lat, Lon) = (a11*w11 + a12*w12 + a21*w21 + a22*w22) / u

Where,

u = w11 + w12 + w21 + w22

c. CRTM calling procedure in the AIT framework

The NWP GFS pressure, temperature, moisture and ozone profiles start on 101 pressure levels.
They are converted to 100 layers in subroutine Compute_Layer_Properties. The layer temperature between two levels is simply the average of the temperature on the two levels.
layer_temperature(i) = (level_temperature(i) + level_temperature(i+1))/2
While pressure, moisture and ozone are assume to be exponential with height.
hp = (log(p1)-log(p2))/(z1-z2)
p = p1* exp(z*hp)
Where p is layer pressure, moisture or ozone. p1,p2 represent level pressure, moisture or ozone. z is the height of the layer.

CRTM needs to be initialized before calling. This is done in subroutine Initialize_OPTRAN. In this call, you tell CRTM which satellite you will run the model. The sensor name is passed through function call CRTM_Init. The sensor name is used to construct the sensor specific SpcCoeff and TauCoeff filenames containing the necessary coefficient data, i.e. seviri_m08.SpcCoeff.bin and seviri_m08.TauCoeff.bin. The sensor names have to match the coefficient file names. You will allocate the output array, which is RTSolution, for the number of channels of the satellite and the number of profiles. You also allocate memory for the CRTM Options, Atmosphere and RTSoluiton structure. Here we allocate the second RTSolution array for the second CRTM call to calculate derivatives for SST algorithm.

Before you call CRTM forward model, load the 100-layer pressure, temperature, Moisture and ozone profiles and the 101 level pressure profile into the Atmosphere Structure. Set the units for the two absorbers (H2O and O3) to be MASS_MIXING_RATIO_UNITS and VOLUME_MIXING_RATIO_UNITS respectively. Set the Water_Coverage in Surface structure to be 100% in order to get surface emissivity over water. Land surface emissivity will be using SEEBOR. Also set other variables in Surface data structure, such as wind speed/direction and surface temperature. Use NWP surface temperature for land and coastline, and OISST sea surface temperature for water. Set Sensor_Zenith_Angle and Source_Zenith_Angle in Geometry structure. Call CRTM_Forward with normal NWP profiles to fill RTSolution, then call CRTM_Forward again with moisture profile multiplied by 1.05 to fill RTSolution_SST. The subroutine for this step is Call_OPTRAN.

After calling CRTM forward model, loop through each channel to calculate transmittance from each level to Top of Atmosphere (TOA). What you get from RTSolution is layer optical depth, to get transmittance

```
 Trans_Atm_Clr(1) = 1.0

 Do Level =  2 , TotalLevels
   Layer_OD = RTSolution(ChnCounter, 1)%Layer_Optical_Depth(Level
-1)
   Layer_OD = Layer_OD /
COS(CRTM%Grid%RTM(LonIndex,LatIndex) &
                    %d(Virtual_ZenAngle_Index)%SatZenAng * DTOR)
   Trans_Atm_Clr(Level) = EXP(-1 * Layer_OD) &
                  * Trans_Atm_Clr(Level - 1)
 ENDDO
```

DTOR is degree to radius PI/180.

Radiance and cloud profiles are calculated in Clear_Radiance_Prof

```
 SUBROUTINE Clear_Radiance_Prof(ChnIndex, TempProf, TauProf,
RadProf, &
                        CloudProf)
 B1 = Planck_Rad_Fast(ChnIndex, TempProf(1))
 RadProf(1) = 0.0_SINGLE
 CloudProf(1) = B1*TauProf(1)

 DO LevelIndex=2, NumLevels
   B2 = Planck_Rad_Fast(ChnIndex, TempProf(LevelIndex))
   dtrn = -(TauProf(LevelIndex) - TauProf(LevelIndex-1))
   RadProf(LevelIndex) = RadProf(LevelIndex-1) +
(B1+B2)/2.0_SINGLE * dtrn


   CloudProf(LevelIndex) = RadProf(LevelIndex) +
B2*TauProf(LevelIndex)
   B1 = B2
 END DO
```

Transmittance, radiance and cloud profiles are calculated for both normal CRTM structure and the 2nd CRTM structure for SST.

Call Clear_Radiance_TOA to get TOA clear-sky radiance and brightness temperature.

```
SUBROUTINE Clear_Radiance_TOA(Option, ChnIndex, RadAtm,
TauAtm, SfcTemp, &
                         SfcEmiss, RadClr, BrTemp_Clr, Rad_Down)
IF(Option == 1) THEN
  IF(PRESENT(Rad_Down))THEN
```

```
    RadClr = RadAtm + (SfcEmiss * Planck_Rad_Fast(ChnIndex,
SfcTemp) &
          + (1. - SfcEmiss) * Rad_Down) * TauAtm
  ELSE
    RadClr = RadAtm + SfcEmiss * Planck_Rad_Fast(ChnIndex,
SfcTemp) &
             * TauAtm
  ENDIF

  CALL Planck_Temp(ChnIndex, RadClr, BrTemp_Clr)

 ELSE
   RadClr = 0.0
   BrTemp_Clr = 0.0
ENDIF
```

In this subroutine, Rad_Down is optional, depending on if you want to have a reflection part from downward radiance when you calculate the clear-sky radiance. Notice that clear-sky radiance and brightness temperature on NWP grid only calculated for normal CRTM structure not the SST CRTM structure.

Also save the downward radiances from RTSolution and RTSolution_SST to CRTM_RadDown and CRTM_RadDown_SST. Save CRTM calculated surface emissivity to CRTM_SfcEmiss. The above steps are done in subroutine CRTM_OPTRAN